An FFT-based adaptive polarization method for infinitely contrasted media with guaranteed convergence

Karam Sab, Jérémy Bleyer, Sébastien Brisard, Martin Dolbeau

An FFT-based adaptive polarization method for infinitely contrasted media with guaranteed convergence

Karam Sab[a], Jérémy Bleyer[a,*], Sébastien Brisard[b], Martin Dolbeau[a]

[a] *Laboratoire Navier, Ecole des Ponts ParisTech, Univ Gustave Eiffel, CNRS, Marne-la-Vallée, France*
[b] *Aix Marseille Univ, CNRS, Centrale Marseille, LMA UMR 7031, Marseille, France*

Abstract

We propose an FFT-based iterative algorithm for solving the Lippmann-Schwinger equation in the context of periodic homogenization of infinitely contrasted linear elastic composites. Our work initially reformulates the Moulinec-Suquet, Eyre-Milton and Monchiet-Bonnet schemes using a residual formulation. Subsequently, we introduce an enhanced scheme, termed Adaptive Eyre–Milton (AEM), as a natural extension of the EM scheme where we optimize a relaxation parameter to minimize the residual. We demonstrate the unconditional linear convergence of the AEM scheme, regardless of initialization and the chosen reference material. The paper further extends the AEM scheme to handle composites with both pores and infinitely rigid inclusions. Practical implementation aspects and illustrative applications in two- and three-dimensional settings are discussed, highlighting the efficiency of the proposed AEM scheme. We particularly emphasize the scheme's robustness for materials with infinitely large contrasts in elastic properties.

Keywords: computational homogenization, FFT-based method, iterative scheme, linear elasticity, composite materials

1. Introduction

Reliably up-scaling the macroscopic behavior of heterogeneous materials with complex microstructures usually requires the full simulation of a boundary value problem (the *homogenization problem*) formulated over the representative volume element. Using classical approaches (e.g. finite elements), these so-called *full-field* simulations often lead to a high numerical cost, both for the discretization of the BVP (meshing of the microstructure) and the solution of the resulting discrete system of equations (large number of unknowns).

Since their first introduction in the mid-nineties by Moulinec and Suquet [1, 2], FFT-based numerical methods have become strong competitors to these standard approaches. The initial corrector problem (a set of partial differential equations) is reformulated as a single integral equation known as the Lippmann–Schwinger equation [3, 4, 5], which is solved iteratively. At each iteration, the convolution kernel of the integral equation must be applied. This is done most efficiently in the Fourier space, by means of fast Fourier transforms (FFT) in a discrete setting.

The first iterative schemes used for the numerical solution of the Lippmann–Schwinger equation were the *basic* scheme of Moulinec and Suquet [1, 2] –referred to as MS in this paper– and the *accelerated* scheme of Eyre and Milton [6] –referred to as EM in the present paper. Both schemes can be seen either as fixed-point iterations of two different operators or, in the case of linear problems, as Neumann-series approximates of the inverses of these operators. Among the "historical" numerical schemes, the *augmented Lagrangian* scheme of Michel, Moulinec and Suquet [7] is also well worth mentioning.

Since these pioneering works, a wealth of new iterative schemes have been introduced, which prove more efficient in some situations, among them the *polarization-based* schemes of Monchiet and Bonnet [8] –referred to as MB in the

*Corresponding author.
Email addresses: karam.sab@enpc.fr (Karam Sab), jeremy.bleyer@enpc.fr (Jérémy Bleyer), sebastien.brisard@univ-amu.fr (Sébastien Brisard), martin.dolbeau@enpc.fr (Martin Dolbeau)

present paper– are important to mention. In a non-linear setting, Newton or quasi-Newton approaches, combined with Krylov solvers [9, 10] deliver very efficient solution schemes [11]. Most notably, by observing that the basic scheme could be seen as a gradient descent, Kabel et al. [12] allowed the introduction of accelerated-gradient methods and other well-known optimization methods [13, 14]. The literature on the topic is very rich, and the reader is referred to the recent and comprehensive review by Schneider [15].

Despite these recent and exciting developments, the MS, EM and MB schemes remain extremely popular. The study [16] focuses on establishing the similarities between these schemes. Introducing the *residual* for these schemes, we in fact realized that they exhibit *almost the same structure*: the difference between MS and EM schemes lies in the increment that is added at each iteration to the residual (we call this increment the *step*). In other words, the EM scheme selects a more efficient step *direction* than the MS scheme, while the MB and the augmented Lagrangian schemes select the same step direction as the EM scheme but with a different step *size*. Keeping the EM step direction unchanged, this observation naturally suggests to *optimize* on a relaxation parameter in order to adapt this step size.

With this idea in mind, we introduce the so-called *adaptive Eyre–Milton* (AEM) scheme. Our experiments indeed confirmed that AEM had a better rate of convergence as MS, EM and MB. More strikingly, we observed that the iterative scheme remains meaningful even in the notoriously difficult case of "doubly infinite contrast" (heterogeneous materials with linear constitutive laws that contain both pores and rigid inclusions). This prompted us to carry out a full mathematical analysis of the newly proposed iterative scheme. This analysis is presented in this work, which is organized as follows.

In Section 2, the homogenization problem in the absence of pores and rigid inclusions is formulated, as well as the corresponding Lippmann–Schwinger equation. Then, the classical formulation of the *basic* MS scheme, the *accelerated* EM scheme and the *polarization-based* MB scheme [8, 17] are recalled.

These three schemes are reformulated in Section 3 in terms of the *residual* that we first define. Our *adaptive Eyre–Milton* scheme (AEM) is then introduced as a natural extension of the EM and MB schemes where we optimize a relaxation parameter λ so as to minimize the residual.

Observing that the AEM scheme remains meaningful for composites with both pores *and* rigid inclusions, it is extended to this case in Section 4. An extended homogenization problem is first introduced and regularity requirements ensuring existence and uniqueness of a solution are stated. Finally, the AEM scheme is formulated in its most general form.

Section 5 is dedicated to the mathematical analysis of the AEM scheme. Our most remarkable result is that this iterative scheme is *unconditionally linearly convergent*. More precisely, the iterations converge to a solution to the homogenization problem *regardless of the initialization and the reference material, and the convergence is linear*.

It is then shown in Section 6 that, for a simple and specific initialization of the iterations, the converged solution can be fully characterized.

This mathematical analysis is followed in Section 7 by the discussion of a few practical issues regarding the implementation of the method, namely: choice of the reference material, initialization, discretization and stopping criteria.

The paper closes in Section 8 with a few illustrative applications, both in a two- and three-dimensional setting. These examples clearly illustrate the performances of the proposed AEM scheme.

2. The homogenization problem

2.1. Presentation

We consider homogenization of a periodic, linearly elastic medium in the d-dimensional real space $\mathbb{R}^d$ ($d = 2, 3$). The unit-cell is denoted by $\Omega = [0, L_1] \times \ldots \times [0, L_d]$ where $L_i > 0$ are the side lengths of Ω and $\langle \bullet \rangle_\Omega$ is the volume average operator over Ω. A field X is Ω-periodic if $X(y_1, \ldots, y_d) = X(y_1 + L_1, \ldots, y_d) = \ldots = X(y_1, \ldots, y_d + L_d)$ at any point $\boldsymbol{y} = (y_1, \ldots, y_d) \in \mathbb{R}^d$.

Let $\boldsymbol{L}^2_{\text{sym}}(\Omega)$ denote the space of symmetric second-order tensor fields $\boldsymbol{y} \mapsto \boldsymbol{e}(\boldsymbol{y})$ ($e_{ij}(\boldsymbol{y}) = e_{ji}(\boldsymbol{y})$, $i, j = 1, \ldots, d$), which are Ω-periodic and square integrable over Ω. Adopting Einstein's summation convention over repeated indices, we introduce the double contraction operator ":" defined as $\boldsymbol{a} : \boldsymbol{b} = a_{ij}\, b_{ij}$, where $\boldsymbol{a}$ and $\boldsymbol{b}$ are two second-order tensors. The bilinear form $(\boldsymbol{a}, \boldsymbol{b}) \mapsto \langle \boldsymbol{a} : \boldsymbol{b} \rangle_\Omega$ then defines a scalar product over $\boldsymbol{L}^2_{\text{sym}}(\Omega)$ and the associated natural norm is

$$\|\boldsymbol{e}\|_{\boldsymbol{L}^2_{\text{sym}}} = \sqrt{\langle \boldsymbol{e} : \boldsymbol{e} \rangle_\Omega}, \tag{1}$$

It is well-known (see e.g. [18]) that, endowed with this natural norm and scalar product, $\boldsymbol{L}^2_{\text{sym}}(\Omega)$ can be decomposed into the two orthogonal sub-spaces $\boldsymbol{S}$ and $\boldsymbol{D}$:

$$\boldsymbol{L}^2_{\text{sym}}(\Omega) = \boldsymbol{S} \overset{\perp}{\oplus} \boldsymbol{D} \tag{2}$$

where $\boldsymbol{S}$ is the sub-space of the $\boldsymbol{e} \in \boldsymbol{L}^2_{\text{sym}}(\Omega)$ which are divergence-free in the sense of distributions over $\mathbb{R}^d$, $e_{ij,j} = 0$, and $\boldsymbol{D}$ is the sub-space of the $\boldsymbol{e} \in \boldsymbol{L}^2_{\text{sym}}(\Omega)$ which are the symmetric part of the gradient of an Ω-periodic displacement vector field $\boldsymbol{u} = (u_i)$, $e_{ij} = \frac{1}{2}(u_{i,j} + u_{j,i})$. Note that uniform fields in $\boldsymbol{L}^2_{\text{sym}}(\Omega)$, like the macroscopic strain $\boldsymbol{E}$, are in S. Actually, for any $\boldsymbol{e}$ in $\boldsymbol{D}$ the corresponding $\boldsymbol{u}$ is unique up to a translation, and it is square integrable over Ω, as well as its gradient. Moreover, the volume-average over Ω of any $\boldsymbol{e}$ in $\boldsymbol{D}$ is null.

Within the framework of linear elasticity, we consider a periodic, heterogeneous material defined by its fourth-order stiffness tensor $\boldsymbol{C}(\boldsymbol{y}) = (C_{ijkl}(\boldsymbol{y}))$ ($\boldsymbol{y} \in \mathbb{R}^d$ and $i, j, k, l = 1, \ldots, d$). The stiffness tensor field $\boldsymbol{C}$ is Ω-periodic and exhibits both minor ($C_{ijkl} = C_{ijlk} = C_{jikl}$) and major ($C_{ijkl} = C_{klij}$) symmetries. Let $\boldsymbol{E}$ denote a macroscopic strain tensor (symmetric, second-order tensor which is uniform over Ω). Then, the homogenization problem reads:

$$\text{Find } \boldsymbol{e}_E \in \boldsymbol{D} \text{ and } \boldsymbol{\sigma}_E \in \boldsymbol{S} \text{ such that } \boldsymbol{\sigma}_E = \boldsymbol{C} : (\boldsymbol{E} + \boldsymbol{e}_E) \tag{3}$$

The above problem has a unique solution, which depends linearly on $\boldsymbol{E}$, if the following condition holds at any point $\boldsymbol{y} \in \Omega$ and for all symmetric second-order tensor $\boldsymbol{e} = (e_{ij})$:

$$\forall \boldsymbol{y} \in \Omega, \;\; m\,\boldsymbol{e} : \boldsymbol{e} \leq \boldsymbol{e} : \boldsymbol{C}(\boldsymbol{y}) : \boldsymbol{e} \leq M\,\boldsymbol{e} : \boldsymbol{e} \tag{4}$$

where $0 < m \leq M$ are two strictly positive scalars. This condition means that both the strain energy density function associated with $\boldsymbol{C}(\boldsymbol{y})$ and the stress energy density function associated with the compliance tensor (inverse of $\boldsymbol{C}(\boldsymbol{y})$) are uniformly coercive in $\boldsymbol{y}$.

Under these conditions, the unique solution to problem (3) (and in particular, the macroscopic stress $\langle \boldsymbol{\sigma} \rangle_\Omega$) depends linearly on the macroscopic strain $\boldsymbol{E}$. The homogenized stiffness tensor $\boldsymbol{C}_{\text{hom}}$ is defined as the linear operator that maps the macroscopic strain onto the macroscopic stress:

$$\langle \boldsymbol{\sigma}_E \rangle_\Omega = \boldsymbol{C}_{\text{hom}} : \boldsymbol{E} \text{ for all } \boldsymbol{E} \tag{5}$$

It is convenient to introduce the fourth-order strain-localization tensor field $\boldsymbol{A}(\boldsymbol{y}) = (A_{ijkl}(\boldsymbol{y}))$. It is defined as the operator that maps the macroscopic strain $\boldsymbol{E}$ onto the microscopic strain $\boldsymbol{\varepsilon}_E(\boldsymbol{y}) = \boldsymbol{E} + \boldsymbol{e}_E(\boldsymbol{y})$:

$$\boldsymbol{\varepsilon}_E(\boldsymbol{y}) = \boldsymbol{A}(\boldsymbol{y}) : \boldsymbol{E}, \quad \text{where} \quad \boldsymbol{\varepsilon}_E(\boldsymbol{y}) = \boldsymbol{E} + \boldsymbol{e}_E(\boldsymbol{y}). \tag{6}$$

Note that $\boldsymbol{A}$ exhibits only minor symmetries ($A_{ijkl} = A_{jikl} = A_{ijlk}$). Then, Eq. (5) leads to the following expression of $\boldsymbol{C}_{\text{hom}}$

$$\boldsymbol{C}_{\text{hom}} = \langle \boldsymbol{C} : \boldsymbol{A} \rangle_\Omega \tag{7}$$

and the following alternative energetic expression can also be derived

$$\boldsymbol{C}_{\text{hom}} = \langle \boldsymbol{A}^t : \boldsymbol{C} : \boldsymbol{A} \rangle_\Omega \tag{8}$$

where $\boldsymbol{A}^t$ is the transpose of $\boldsymbol{A}$ defined by $A^t_{ijkl} = A_{klij}$.

In the remainder of this paper, $\boldsymbol{C}_0$ denotes an arbitrary reference material, which is a uniform, positive-definite ($\boldsymbol{e} : \boldsymbol{C}_0 : \boldsymbol{e} > 0$ for all $\boldsymbol{e} \neq 0$), fourth-order tensor with both minor and major symmetries. Let m_0 and M_0 be respectively the smallest and largest eigenvalues of $\boldsymbol{C}_0$ ($0 < m_0 \leq M_0$). Then, from (4), one can easily obtain the following equivalent uniform coercivity condition:

$$\forall \boldsymbol{y} \in \Omega, \;\; \mu^- \boldsymbol{e} : \boldsymbol{C}_0 : \boldsymbol{e} \leq \boldsymbol{e} : \boldsymbol{C}(\boldsymbol{y}) : \boldsymbol{e} \leq \mu^+ \boldsymbol{e} : \boldsymbol{C}_0 : \boldsymbol{e} \tag{9}$$

where $\mu^- = m/M_0 > 0$ and $\mu^+ = M/m_0 > 0$. Moreover, the $\boldsymbol{C}_0$-norm is defined over $\boldsymbol{L}^2_{\text{sym}}(\Omega)$ as follows:

$$\|\boldsymbol{e}\|_{\boldsymbol{C}_0} = \sqrt{\langle \boldsymbol{e} : \boldsymbol{C}_0 : \boldsymbol{e} \rangle_\Omega} \tag{10}$$

Owing to the symmetry and positive definiteness of $\boldsymbol{C}_0$, the $\boldsymbol{C}_0$-norm $\|\bullet\|_{\boldsymbol{C}_0}$ is equivalent to the natural norm $\|\bullet\|_{\boldsymbol{L}^2_{\mathrm{sym}}}$. Indeed, we have:

$$m_0 \|\boldsymbol{e}\|^2_{\boldsymbol{L}^2_{\mathrm{sym}}} \leq \|\boldsymbol{e}\|^2_{\boldsymbol{C}_0} \leq M_0 \|\boldsymbol{e}\|^2_{\boldsymbol{L}^2_{\mathrm{sym}}} \tag{11}$$

For any $\boldsymbol{\tau} \in \boldsymbol{L}^2_{\mathrm{sym}}(\Omega)$, the following problem

$$\text{Find } \boldsymbol{e}_\tau \in \boldsymbol{D} \text{ such that } \boldsymbol{C}_0 : \boldsymbol{e}_\tau + \boldsymbol{\tau} \in \boldsymbol{S} \tag{12}$$

has a unique solution $\boldsymbol{e}_\tau$ that depends linearly on $\boldsymbol{\tau}$. The Green operator $\boldsymbol{\Gamma}^0$ associated to $\boldsymbol{C}_0$ is defined as the linear operator that maps $\boldsymbol{\tau}$ onto $-\boldsymbol{e}_\tau$ [3, 4, 5]:

$$\boldsymbol{e}_\tau = -\boldsymbol{\Gamma}^0 * \boldsymbol{\tau} \tag{13}$$

The Green operator $\boldsymbol{\Gamma}^0$ has an analytical expression in Fourier space, and hence the convolution $\boldsymbol{\Gamma}^0 * \boldsymbol{\tau}$ can be efficiently computed using FFT techniques [1, 2]. The $\boldsymbol{\Gamma}^0$ operator thus defined enjoys a number of properties [7]:

$$\boldsymbol{\Gamma}^0 * \boldsymbol{\tau} = 0 \quad \Longleftrightarrow \quad \boldsymbol{\tau} \in \boldsymbol{S} \tag{14}$$

$$\langle \boldsymbol{e} : \boldsymbol{C}_0 : (\boldsymbol{\Gamma}^0 * \boldsymbol{\tau}) \rangle_\Omega = \langle \boldsymbol{e} : \boldsymbol{\tau} \rangle_\Omega \text{ for all } \boldsymbol{\tau} \in \boldsymbol{L}^2_{\mathrm{sym}}(\Omega) \text{ and } \boldsymbol{e} \in \boldsymbol{D}. \tag{15}$$

In particular, inserting $\boldsymbol{e} = \boldsymbol{\Gamma}^0 * \boldsymbol{\tau}$ in the above equation and using the Cauchy-Schwartz inequality shows that the linear map $\boldsymbol{\tau} \mapsto \boldsymbol{\Gamma}^0 * \boldsymbol{\tau}$ is continuous from $\boldsymbol{L}^2_{\mathrm{sym}}(\Omega)$ to $\boldsymbol{D}$.

It is a classical result that, under the uniform coercivity condition (4), the homogenization problem (3) is equivalent to the following Lippmann–Schwinger equation

$$\boldsymbol{\varepsilon} = \boldsymbol{E} - \boldsymbol{\Gamma}^0 * [(\boldsymbol{C} - \boldsymbol{C}_0) : \boldsymbol{\varepsilon}] \tag{16}$$

where $\boldsymbol{C}_0$ and $\boldsymbol{\Gamma}^0$ are defined above (see also [19, 20, 2]). Indeed, the unique solution $\boldsymbol{\varepsilon}_E$ to the above equation is such that $\boldsymbol{\varepsilon}_E = \boldsymbol{E} + \boldsymbol{e}_E$, where $\boldsymbol{e}_E$ is the unique solution to the homogenization problem (3).

To close this section, we introduce a decomposition of any tensor field in $\boldsymbol{L}^2_{\mathrm{sym}}(\Omega)$; this decomposition will play a crucial role in the developments below (see also [21]). For all $\boldsymbol{e} \in \boldsymbol{L}^2_{\mathrm{sym}}(\Omega)$, we define:

$$\boldsymbol{e}^D = \boldsymbol{\Gamma}^0 * (\boldsymbol{C}_0 : \boldsymbol{e}) \quad \text{and} \quad \boldsymbol{e}^S = \boldsymbol{e} - \boldsymbol{e}^D \tag{17}$$

with the following properties:

$$\boldsymbol{e}^D \in \boldsymbol{D}, \quad \boldsymbol{C}_0 : \boldsymbol{e}^S \in \boldsymbol{S} \quad \text{and} \quad \|\boldsymbol{e}\|^2_{\boldsymbol{C}_0} = \|\boldsymbol{e}^D\|^2_{\boldsymbol{C}_0} + \|\boldsymbol{e}^S\|^2_{\boldsymbol{C}_0} \tag{18}$$

and

$$\langle \boldsymbol{e}_1 : \boldsymbol{C}_0 : \boldsymbol{e}_2^S \rangle_\Omega = \langle \boldsymbol{e}_1^S : \boldsymbol{C}_0 : \boldsymbol{e}_2 \rangle_\Omega \quad \text{and} \quad \langle \boldsymbol{e}_1 : \boldsymbol{C}_0 : \boldsymbol{e}_2^D \rangle_\Omega = \langle \boldsymbol{e}_1^D : \boldsymbol{C}_0 : \boldsymbol{e}_2 \rangle_\Omega, \tag{19}$$

for all $\boldsymbol{e}_1, \boldsymbol{e}_2 \in \boldsymbol{L}^2_{\mathrm{sym}}(\Omega)$.

Hence, $\boldsymbol{e}^D$ appears as the orthogonal projection of $\boldsymbol{e}$ on $\boldsymbol{D}$ with respect to the $\boldsymbol{C}_0$-norm. Using the orthogonal decomposition (2) with respect to the $\boldsymbol{L}^2_{\mathrm{sym}}$-norm, it is seen that the orthogonal of $\boldsymbol{D}$ with respect to the $\boldsymbol{C}_0$-norm is the subspace of $\boldsymbol{e}' \in \boldsymbol{L}^2_{\mathrm{sym}}(\Omega)$ such that $\langle \boldsymbol{e} : \boldsymbol{C}_0 : \boldsymbol{e}' \rangle_\Omega = 0$ for any $\boldsymbol{e} \in \boldsymbol{D}$, i.e. $\boldsymbol{C}_0 : \boldsymbol{e}' \in \boldsymbol{S}$. Therefore, unless $\boldsymbol{C}_0$ is of the form $k\boldsymbol{I}$, with k a positive scalar and $\boldsymbol{I}$ the fourth-order identity tensor operating on symmetric second order tensors ($\boldsymbol{I} : \boldsymbol{e} = \boldsymbol{e}$ for any symmetric second order tensor $\boldsymbol{e}$), the subspaces $\boldsymbol{D}$ and $\boldsymbol{S}$ are *not* orthogonal with respect to the $\boldsymbol{C}_0$-norm, $\boldsymbol{e}^S = \boldsymbol{e} - \boldsymbol{e}^D$ is *not* in $\boldsymbol{S}$ and it is *not* the orthogonal projection of $\boldsymbol{e}$ on $\boldsymbol{S}$ with respect to the $\boldsymbol{C}_0$-norm. $\boldsymbol{e}^S$ is actually the projection (with respect to the $\boldsymbol{C}_0$-norm) of $\boldsymbol{e}$ on the subspace of $\boldsymbol{e}' \in \boldsymbol{L}^2_{\mathrm{sym}}(\Omega)$ such that $\boldsymbol{C}_0 : \boldsymbol{e}' \in \boldsymbol{S}$. Moreover, combining (14) with (17), we obtain the following characterizations of $\boldsymbol{S}$ and $\boldsymbol{D}$:

$$(\boldsymbol{C}_0^{-1} : \boldsymbol{\tau})^D = 0 \quad \Longleftrightarrow \quad \boldsymbol{\tau} \in \boldsymbol{S}, \quad \text{and} \quad \boldsymbol{e}^S = 0 \quad \Longleftrightarrow \quad \boldsymbol{e} \in \boldsymbol{D}. \tag{20}$$

As a result, the $\boldsymbol{C}_0$-norm of $(\boldsymbol{C}_0^{-1} : \boldsymbol{\tau})^D$ can be considered as a measure of the equilibrium error for the stress field $\boldsymbol{\tau}$ and the $\boldsymbol{C}_0$-norm of $\boldsymbol{e}^S$ can be considered as a measure of the compatibility error for the strain field $\boldsymbol{e}$.

It should be emphasized that multiplying $\boldsymbol{C}_0$ by a strictly positive real does not change the above introduced decomposition.

2.2. *The Moulinec–Suquet, Eyre–Milton and Monchiet–Bonnet schemes*

The Lippmann–Schwinger equation (16) is at the center of the so-called "FFT-based numerical homogenization techniques" first introduced by Moulinec and Suquet [1, 2]. The reader is referred to the recent review [15] for a more detailed description of this numerical technique. Regardless of the spatial discretization, this equation must be solved iteratively. Since the early works of Moulinec and Suquet, much attention has been devoted to comparing the merits (in particular, number of iterations to convergence) of various iterative solvers [6, 7, 8, 16, 13, 14, 17]. In the present section, we focus on the so-called "basic" scheme [1, 2], the "accelerated" Eyre–Milton scheme [6] and the "polarization-based" Monchiet–Bonnet scheme [8, 17] that we cast in a similar form where the *residual* is explicit. Our adaptive scheme (introduced in Section 3) will then appear as a clear and natural extension to the Eyre–Milton scheme.

In the "basic scheme", Moulinec and Suquet make use of the following fixed-point iterations [1, 2]

$$\begin{cases} \textbf{Initialization} \\ \quad \boldsymbol{\varepsilon}^0 = \boldsymbol{E} \end{cases} \quad \text{and} \quad \begin{cases} \textbf{Iterations } (n \geq 0) \\ \boldsymbol{\varepsilon}^{n+1} = \boldsymbol{E} - \boldsymbol{\Gamma}^0 * [(\boldsymbol{C} - \boldsymbol{C}_0) : \boldsymbol{\varepsilon}^n] \end{cases} \tag{21}$$

When all constituents (including the reference material) are isotropic, Michel et al. [7] showed that the above iterations converge under the following sufficient condition:

$$0 < K(\boldsymbol{y}) < 2K_0 \quad \text{and} \quad 0 < G(\boldsymbol{y}) < 2G_0 \quad \text{for all } \boldsymbol{y} \in \Omega, \tag{22}$$

where K_0 and G_0 (resp. $K(\boldsymbol{y})$ and $G(\boldsymbol{y})$) are the bulk and shear moduli of the reference material (resp. the material at point $\boldsymbol{y}$). The recommended bulk and shear moduli of the reference material are:

$$K_0 = \tfrac{1}{2}(K_{\min} + K_{\max}) \quad \text{and} \quad G_0 = \tfrac{1}{2}(G_{\min} + G_{\max}), \tag{23}$$

where $K_{\min}$ and $K_{\max}$ (resp. $G_{\min}$ and $G_{\max}$) denote the minimum and maximum bulk (resp. shear) moduli over Ω.

It has been shown theoretically [7, 16] that the number of iterations to convergence grows as the mechanical contrast $\chi = \max\{K_{\max}/K_{\min}, G_{\max}/G_{\min}\}$. Although the MS scheme converges for porous materials with a suitable pore distribution, in the general case, the number of iterations to convergence becomes unacceptably large for large contrasts.

Eyre and Milton [6] later introduced a modified scheme that converges considerably faster than the basic scheme in some cases, see [22] for a comparison between these two schemes. This iterative scheme was recast by Moulinec and Silva [16] as follows:

$$\begin{cases} \textbf{Initialization} \\ \quad \boldsymbol{\varepsilon}^0 = \boldsymbol{E} \end{cases} \quad \text{and} \quad \begin{cases} \textbf{Iterations } (n \geq 0) \\ \boldsymbol{\varepsilon}^{n+1} = \boldsymbol{\varepsilon}^n + \boldsymbol{\alpha} : \left(\boldsymbol{E} - \boldsymbol{\varepsilon}^n - \boldsymbol{\Gamma}^0 * [(\boldsymbol{C} - \boldsymbol{C}_0) : \boldsymbol{\varepsilon}^n]\right) \end{cases} \tag{24}$$

where $\boldsymbol{\alpha}$ is the fourth-order tensor field given by:

$$\boldsymbol{\alpha}(\boldsymbol{y}) = 2(\boldsymbol{C}(\boldsymbol{y}) + \boldsymbol{C}_0)^{-1} : \boldsymbol{C}_0 \tag{25}$$

Note that the basic scheme is recovered upon substituting formally $\boldsymbol{\alpha}(\boldsymbol{y})$ with $\boldsymbol{I}$. When all constituents are isotropic, a sufficient convergence condition was established by Michel et al. [7] and further investigated by Moulinec and Silva [16]. The recommended bulk and shear moduli of the reference material are now:

$$K_0 = \sqrt{K_{\min} K_{\max}} \quad \text{and} \quad G_0 = \sqrt{G_{\min} G_{\max}} \tag{26}$$

The EM iterations are significantly faster in some cases than the MS iterations. Indeed, the number of EM iterations to convergence grows as $\sqrt{\chi}$ (square root of the mechanical contrast), rather than χ for the MS iterations [7, 16, 17]. These are actually bounds and (like MS) the EM scheme does converge for porous materials. Nevertheless, in the general case, the number of iterations increases with the contrast and may become unacceptable in some cases.

As for the polarization-based scheme, it was first proposed by Monchiet and Bonnet [8] and recast by Moulinec and Silva, see eq. (13) in [16]. A straightforward manipulation of this equation gives the following expression of the iterations ($n \geq 0$):

$$\boldsymbol{\varepsilon}^{n+1} = \boldsymbol{\varepsilon}^n + \lambda_1 \boldsymbol{\alpha} : \left(\boldsymbol{E} - \boldsymbol{\varepsilon}^n + \boldsymbol{\Gamma}^0 * [\boldsymbol{C}_0 : \boldsymbol{\varepsilon}^n]\right) - \lambda_2 \boldsymbol{\alpha} : \left(\boldsymbol{\Gamma}^0 * [\boldsymbol{C} : \boldsymbol{\varepsilon}^n]\right) \tag{27}$$

where λ_1 and λ_2 are two constants (corresponding to, respectively, $\alpha/2$ and $\beta/2$ in eq. (13) of [16]). In all existing studies λ_1 and λ_2 are taken equal to a common value λ leading to the iterations ($n \geq 0$):

$$\boldsymbol{\varepsilon}^{n+1} = \boldsymbol{\varepsilon}^n + \lambda \boldsymbol{\alpha} : \left(\boldsymbol{E} - \boldsymbol{\varepsilon}^n - \boldsymbol{\Gamma}^0 * [(\boldsymbol{C} - \boldsymbol{C}_0) : \boldsymbol{\varepsilon}^n] \right) \tag{28}$$

Moreover, the above polarization-based scheme can be interpreted as a Douglas–Rachford splitting [17]. λ is actually equal to $1 - \gamma$ where γ in [17] is the damping parameter with the condition $\gamma \in [0, 1)$. As pointed out in [8], [16] and [17], this scheme appears as an extension of the Eyre–Milton scheme which is recovered for $\gamma = 0$ ($\lambda = 1$). Also, the augmented Lagrangian scheme [7] corresponds to $\gamma = 1/2$ ($\lambda = 1/2$) and Monchiet–Bonnet [8] recommend using $\gamma = 1/4$ ($\lambda = 3/4$) based on a series of numerical experiments.

Another important feature in [17] is to adopt zero initialization leading to the following scheme:

$$\begin{cases} \textbf{Initialization} \\ \boldsymbol{\varepsilon}^0 = 0 \end{cases} \quad \text{and} \quad \begin{cases} \textbf{Iterations } (n \geq 0) \\ \boldsymbol{\varepsilon}^{n+1} = \boldsymbol{\varepsilon}^n + (1-\gamma)\boldsymbol{\alpha} : \left(\boldsymbol{E} - \boldsymbol{\varepsilon}^n - \boldsymbol{\Gamma}^0 * [(\boldsymbol{C} - \boldsymbol{C}_0) : \boldsymbol{\varepsilon}^n] \right) \end{cases} \tag{29}$$

It was proved by Schneider et al. [17] that the convergence properties of all polarization-based schemes were qualitatively the same. In particular, the number of iterations to convergence grows as $\sqrt{\chi}$ like the EM iterations. In the following, we will refer to (29) as γ-polarization schemes. We distinguish in particular the original Eyre-Milton scheme (EM) (24) from the $\gamma = 0$-polarization scheme as the latter involves a different initialization than the former despite identical iteration relations.

3. The Adaptive Eyre–Milton scheme (AEM)

In order to introduce our adaptive scheme, we first rewrite the MS and EM schemes in terms of the *residual* $\boldsymbol{X}^n$, defined as follows in both cases

$$\boldsymbol{X}^n = \boldsymbol{E} - \boldsymbol{\varepsilon}^n - \boldsymbol{\Gamma}^0 * [(\boldsymbol{C} - \boldsymbol{C}_0) : \boldsymbol{\varepsilon}^n] \tag{30}$$

It is readily verified that the MS scheme, see Eq. (21), is equivalent to

$$\begin{cases} \textbf{Initialization} \\ \boldsymbol{\varepsilon}^0 = \boldsymbol{E} \\ \boldsymbol{X}^0 = -\boldsymbol{\Gamma}^0 * [(\boldsymbol{C} - \boldsymbol{C}_0) : \boldsymbol{E}] \end{cases} \quad \text{and} \quad \begin{cases} \textbf{Iterations } (n \geq 0) \\ \boldsymbol{\varepsilon}^{n+1} = \boldsymbol{\varepsilon}^n + \boldsymbol{X}^n \\ \boldsymbol{Z}^n = \boldsymbol{X}^n + \boldsymbol{\Gamma}^0 * [(\boldsymbol{C} - \boldsymbol{C}_0) : \boldsymbol{X}^n] \\ \boldsymbol{X}^{n+1} = \boldsymbol{X}^n - \boldsymbol{Z}^n \end{cases} \tag{31}$$

while it is proved in Appendix A that the EM scheme, see Eq. (24), can be reformulated as follows

$$\begin{cases} \textbf{Initialization} \\ \boldsymbol{\varepsilon}^0 = \boldsymbol{E} \\ \boldsymbol{X}^0 = -\boldsymbol{\Gamma}^0 * [(\boldsymbol{C} - \boldsymbol{C}_0) : \boldsymbol{E}] \end{cases} \quad \text{and} \quad \begin{cases} \textbf{Iterations } (n \geq 0) \\ \boldsymbol{\varepsilon}^{n+1} = \boldsymbol{\varepsilon}^n + \boldsymbol{\alpha} : \boldsymbol{X}^n \\ \boldsymbol{Z}^n = \boldsymbol{\alpha} : \boldsymbol{X}^n + \boldsymbol{\Gamma}^0 * [(\boldsymbol{C} - \boldsymbol{C}_0) : \boldsymbol{\alpha} : \boldsymbol{X}^n] \\ \boldsymbol{X}^{n+1} = \boldsymbol{X}^n - \boldsymbol{Z}^n \end{cases} \tag{32}$$

This alternative formulation shows the striking similarities between the two schemes, where $\boldsymbol{Z}^n$ appears as the iteration step. Both MS and EM methods can therefore be seen as *fixed-step* iterative methods. We introduce in the present section some adaptivity by means of the relaxation parameter λ^n

$$\boldsymbol{\varepsilon}^{n+1} = \boldsymbol{\varepsilon}^n + \lambda^n \, \boldsymbol{\alpha} : \boldsymbol{X}^n \quad \text{and} \quad \boldsymbol{X}^{n+1} = \boldsymbol{X}^n - \lambda^n \, \boldsymbol{Z}^n \tag{33}$$

where λ^n is selected so as to minimize the next residual $\boldsymbol{X}^{n+1}$. The issue which arises naturally is the best choice for the residual norm. After many attempts, we have found that the $\boldsymbol{C}_0$-norm guarantees the *linear convergence* of the scheme for all $\boldsymbol{C}_0$ (see proof in Section 5):

$$\lambda^n = \underset{\lambda \in \mathbb{R}}{\arg\min} \, \|\boldsymbol{X}^n - \lambda \, \boldsymbol{Z}^n\|_{\boldsymbol{C}_0} \quad \Longleftrightarrow \quad \lambda^n = \frac{\langle \boldsymbol{X}^n : \boldsymbol{C}_0 : \boldsymbol{Z}^n \rangle_\Omega}{\langle \boldsymbol{Z}^n : \boldsymbol{C}_0 : \boldsymbol{Z}^n \rangle_\Omega} \tag{34}$$

We call the resulting iterative scheme the *Adaptive Eyre–Milton* scheme (AEM). Differing discussion of the initialization to Section 6.1, the proposed scheme reads

$$\left\{\begin{aligned} &\textbf{Iterations } (n \geq 0)\\ \boldsymbol{Z}^n &= \boldsymbol{\alpha} : \boldsymbol{X}^n + \boldsymbol{\Gamma}^0 * [(\boldsymbol{C} - \boldsymbol{C}_0) : \boldsymbol{\alpha} : \boldsymbol{X}^n]\\ \lambda^n &= \frac{\langle \boldsymbol{X}^n : \boldsymbol{C}_0 : \boldsymbol{Z}^n \rangle_\Omega}{\langle \boldsymbol{Z}^n : \boldsymbol{C}_0 : \boldsymbol{Z}^n \rangle_\Omega}\\ \boldsymbol{\varepsilon}^{n+1} &= \boldsymbol{\varepsilon}^n + \lambda^n \boldsymbol{\alpha} : \boldsymbol{X}^n\\ \boldsymbol{X}^{n+1} &= \boldsymbol{X}^n - \lambda^n \boldsymbol{Z}^n \end{aligned}\right. \tag{35}$$

It is extremely fruitful to rewrite the above iterations in terms of the following fourth-order tensor fields:

$$\boldsymbol{C}^D(\boldsymbol{y}) = \boldsymbol{C}(\boldsymbol{y}) : \boldsymbol{\alpha}(\boldsymbol{y}) = 2\boldsymbol{C}(\boldsymbol{y}) : (\boldsymbol{C}(\boldsymbol{y}) + \boldsymbol{C}_0)^{-1} : \boldsymbol{C}_0 \tag{36}$$

$$\boldsymbol{C}^S(\boldsymbol{y}) = \boldsymbol{C}_0 : \boldsymbol{\alpha} = 2\boldsymbol{C}_0 : (\boldsymbol{C}(\boldsymbol{y}) + \boldsymbol{C}_0)^{-1} : \boldsymbol{C}_0 \tag{37}$$

Both $\boldsymbol{C}^D(\boldsymbol{y})$ and $\boldsymbol{C}^S(\boldsymbol{y})$ have the minor symmetries and $\boldsymbol{C}^S(\boldsymbol{y})$ clearly has the major symmetry. Further observing that

$$\boldsymbol{C}^D(\boldsymbol{y}) + \boldsymbol{C}^S(\boldsymbol{y}) = 2\boldsymbol{C}_0 \tag{38}$$

delivers the major symmetry of $\boldsymbol{C}^D(\boldsymbol{y})$. Therefore, both $\boldsymbol{C}^D(\boldsymbol{y})$ and $\boldsymbol{C}^S(\boldsymbol{y})$ exhibit the symmetries of elasticity tensors. The following bounds on $\boldsymbol{C}^D(\boldsymbol{y})$ and $\boldsymbol{C}^S(\boldsymbol{y})$ are proved in Appendix B. These bounds result from the uniform coercivity condition (9) and hold for all symmetric second-order tensor $\boldsymbol{e} = (e_{ij})$ and all $\boldsymbol{y} \in \Omega$:

$$0 < \boldsymbol{e} : \boldsymbol{C}^{D-} : \boldsymbol{e} \leq \boldsymbol{e} : \boldsymbol{C}^D(\boldsymbol{y}) : \boldsymbol{e} \leq \boldsymbol{e} : \boldsymbol{C}^{D+} : \boldsymbol{e} < \boldsymbol{e} : 2\boldsymbol{C}_0 : \boldsymbol{e}, \tag{39}$$

$$0 < \boldsymbol{e} : \boldsymbol{C}^{S-} : \boldsymbol{e} \leq \boldsymbol{e} : \boldsymbol{C}^S(\boldsymbol{y}) : \boldsymbol{e} \leq \boldsymbol{e} : \boldsymbol{C}^{S+} : \boldsymbol{e} < \boldsymbol{e} : 2\boldsymbol{C}_0 : \boldsymbol{e} \tag{40}$$

where

$$\boldsymbol{C}^{D\pm} = 2\boldsymbol{C}_0 - \boldsymbol{C}^{S\mp}, \quad \boldsymbol{C}^{S-} = \frac{2}{1+\mu^+}\boldsymbol{C}_0, \quad \boldsymbol{C}^{S+} = \frac{2}{1+\mu^-}\boldsymbol{C}_0. \tag{41}$$

Hence, upon initializing the scheme with some $\boldsymbol{\varepsilon}^0$ and its corresponding residual $\boldsymbol{X}^0$, the proposed AEM scheme (35) becomes:

$$\left\{\begin{aligned} &\textbf{Iterations } (n \geq 0)\\ \boldsymbol{Z}^n &= \boldsymbol{\alpha} : \boldsymbol{X}^n + \boldsymbol{\Gamma}^0 * [(\boldsymbol{C}^D - \boldsymbol{C}^S) : \boldsymbol{X}^n]\\ \lambda^n &= \frac{\langle \boldsymbol{X}^n : \boldsymbol{C}_0 : \boldsymbol{Z}^n \rangle_\Omega}{\langle \boldsymbol{Z}^n : \boldsymbol{C}_0 : \boldsymbol{Z}^n \rangle_\Omega}\\ \boldsymbol{\varepsilon}^{n+1} &= \boldsymbol{\varepsilon}^n + \lambda^n \boldsymbol{\alpha} : \boldsymbol{X}^n\\ \boldsymbol{X}^{n+1} &= \boldsymbol{X}^n - \lambda^n \boldsymbol{Z}^n \end{aligned}\right. \tag{42}$$

It is remarkable that the above reformulation of our Adaptive Eyre–Milton scheme remains meaningful for microstructures that contain pores ($\boldsymbol{C} \to 0$) and/or rigid inclusions ($\boldsymbol{C} \to \infty$). Indeed, in these extreme cases, $\boldsymbol{\alpha}$ and the "pseudo elasticity tensors" $\boldsymbol{C}^D$ and $\boldsymbol{C}^S$ remain well-defined (and finite). This observation suggests to formally extend the iterative scheme (42) to periodic composite materials containing several non-intersecting rigid inclusions and pores which have sufficiently smooth boundaries.

4. AEM scheme for composites containing pores and rigid inclusions

Let Ω^{r}, Ω^{p} and Ω^{m} denote the open domains of Ω occupied by, respectively, the rigid inclusions, the pores and the heterogeneous matrix. The Ω-periodic stiffness tensor field $\boldsymbol{C}(\boldsymbol{y})$ is defined only for $\boldsymbol{y} \in \Omega^{\mathrm{m}}$. Whereas, the Ω-periodic tensor fields $\boldsymbol{\alpha}(\boldsymbol{y})$, $\boldsymbol{C}^S(\boldsymbol{y})$ and $\boldsymbol{C}^D(\boldsymbol{y})$ are defined over the whole unit cell as follows:

$$\forall \boldsymbol{y} \in \Omega^{\mathrm{r}}: \quad \boldsymbol{\alpha}(\boldsymbol{y}) = 0, \qquad \boldsymbol{C}^S(\boldsymbol{y}) = 0, \qquad \boldsymbol{C}^D(\boldsymbol{y}) = 2\boldsymbol{C}_0, \tag{43}$$

$$\forall \boldsymbol{y} \in \Omega^{\mathrm{p}}: \quad \boldsymbol{\alpha}(\boldsymbol{y}) = 2\boldsymbol{I}, \qquad \boldsymbol{C}^S(\boldsymbol{y}) = 2\boldsymbol{C}_0, \qquad \boldsymbol{C}^D(\boldsymbol{y}) = 0, \tag{44}$$

$$\forall \boldsymbol{y} \in \Omega^{\mathrm{m}}: \quad \boldsymbol{\alpha}(\boldsymbol{y}) = 2(\boldsymbol{C}(\boldsymbol{y}) + \boldsymbol{C}_0)^{-1} : \boldsymbol{C}_0, \quad \boldsymbol{C}^S(\boldsymbol{y}) = 2\boldsymbol{C}_0 : (\boldsymbol{C}(\boldsymbol{y}) + \boldsymbol{C}_0)^{-1} : \boldsymbol{C}_0, \quad \boldsymbol{C}^D(\boldsymbol{y}) = \boldsymbol{C}(\boldsymbol{y}) : \boldsymbol{\alpha}(\boldsymbol{y}). \tag{45}$$

The tensors $\boldsymbol{\alpha}$, $\boldsymbol{C}^D$ and $\boldsymbol{C}^S$ being defined over the whole unit-cell Ω, the iterations (42) can be performed. Two questions then arise: (1) does the iterative scheme converge and, if yes, (2) what is the converged field $\lim_{n\to\infty} \boldsymbol{\varepsilon}^n$.

It is proved in Section 5, that, under mild conditions on the coercivity of $\boldsymbol{C}$ and the regularity of the domains Ω^{r}, and Ω^{p}, the iterative scheme (42) is indeed linearly convergent. Besides, the sequence of $\boldsymbol{\varepsilon}^n$ converges to the solution to a well-posed homogenization problem that extends (3) and which is introduced in the following.

4.1. The extended homogenization problem

For heterogeneous materials containing pores and rigid inclusions, it is expected that the stress is null in the pores and the strain is null in the rigid inclusions, while stresses and strains are associated by the heterogeneous elasticity tensor $\boldsymbol{C}$ anywhere else in the unit cell. Hence, in such materials, the constitutive equations must be modified as follows. We say that a pair of strain-stress fields, $(\boldsymbol{\varepsilon}, \boldsymbol{\sigma}) \in \boldsymbol{L}^2_{\mathrm{sym}}(\Omega) \times \boldsymbol{L}^2_{\mathrm{sym}}(\Omega)$, complies to the constitutive equations if the following equations hold true:

$$\boldsymbol{\varepsilon} = 0 \text{ in } \Omega^{\mathrm{r}}, \quad \boldsymbol{\sigma} = 0 \text{ in } \Omega^{\mathrm{p}} \quad \text{and} \quad \boldsymbol{\sigma} = \boldsymbol{C} : \boldsymbol{\varepsilon} \text{ in } \Omega^{\mathrm{m}}. \tag{46}$$

Then, the homogenization problem (3) must be modified as follows:

$$\text{Find } (\boldsymbol{e}_E, \boldsymbol{\sigma}_E) \in \boldsymbol{D} \times \boldsymbol{S} \text{ such that } (\boldsymbol{\varepsilon}_E = \boldsymbol{E} + \boldsymbol{e}_E, \boldsymbol{\sigma}_E) \text{ complies to (46)} \tag{47}$$

It is shown that under the assumptions stated in Section 4.2, that the above problem has a unique solution, $(\boldsymbol{\varepsilon}_E, \boldsymbol{\sigma}_E)$, up to a pair $(\boldsymbol{e}, \boldsymbol{\sigma}) \in \boldsymbol{D} \times \boldsymbol{S}$ with $(\boldsymbol{e}, \boldsymbol{\sigma}) = (0, 0)$ in Ω^{m}. In other words, the localization tensor $\boldsymbol{A}$ introduced in (6) is uniquely defined in Ω^{m}. Hence, the homogenized stiffness tensor becomes:

$$\boldsymbol{C}_{\mathrm{hom}} = \frac{|\Omega^{\mathrm{m}}|}{|\Omega|} \langle \boldsymbol{A}^t : \boldsymbol{C} : \boldsymbol{A} \rangle_{\Omega^{\mathrm{m}}} \tag{48}$$

The definition of the residual must be slightly modified as follows: for any pair of strain-stress fields $(\boldsymbol{\varepsilon}, \boldsymbol{\sigma}) \in \boldsymbol{L}^2_{\mathrm{sym}}(\Omega) \times \boldsymbol{L}^2_{\mathrm{sym}}(\Omega)$ complying to the constitutive equations (46), the corresponding residual field $\boldsymbol{X}(\boldsymbol{y})$ is defined by:

$$\boldsymbol{X} = \boldsymbol{E} - \boldsymbol{\varepsilon} - \boldsymbol{\Gamma}^0 * [(\boldsymbol{\sigma} - \boldsymbol{C}_0 : \boldsymbol{\varepsilon}], \tag{49}$$

Actually, $\boldsymbol{X} = 0$ if, and only if, $(\boldsymbol{\varepsilon}, \boldsymbol{\sigma})$ is a solution of the homogenization problem. Indeed, by definition, we have $\boldsymbol{\varepsilon}^D = \boldsymbol{\Gamma}^0 * [\boldsymbol{C}_0 : \boldsymbol{\varepsilon}]$, and $\boldsymbol{X}$ can be decomposed as:

$$\boldsymbol{X} = \boldsymbol{X}^S + \boldsymbol{X}^D \text{ with } \boldsymbol{X}^S = \boldsymbol{E} - \boldsymbol{\varepsilon}^S = (\boldsymbol{E} - \boldsymbol{\varepsilon})^S \text{ and } \boldsymbol{X}^D = -\boldsymbol{\Gamma}^0 * \boldsymbol{\sigma} = -\left(\boldsymbol{C}_0^{-1} : \boldsymbol{\sigma}\right)^D. \tag{50}$$

The conclusion is obtained by noticing that $\boldsymbol{X} = 0$ is equivalent to $\boldsymbol{X}^D = 0$ and $\boldsymbol{X}^S = 0$, and that $\boldsymbol{X}^D = 0$ is equivalent to $\boldsymbol{\sigma} \in \boldsymbol{S}$ and $\boldsymbol{X}^S = 0$ is equivalent to $\boldsymbol{\varepsilon} = \boldsymbol{E} + \boldsymbol{\varepsilon}^D$.

The fact that the strain field is null over Ω^{r} and the stress field is null over Ω^{p} leads to remarkable properties of $\boldsymbol{X}^S$ and $\boldsymbol{X}^D$ which are described in the following.

Characterizing $\boldsymbol{X}^S$ in the rigid inclusions. Note that, by definition, $\boldsymbol{C}_0 : \boldsymbol{X}^S$ is divergence-free in the whole Ω. Moreover, the restriction of $\boldsymbol{X}^S$ to Ω^{r} is given by $\boldsymbol{X}^S = \boldsymbol{E} - \boldsymbol{\varepsilon}^S = \boldsymbol{E} + \boldsymbol{\varepsilon}^D$ because $\boldsymbol{\varepsilon} = \boldsymbol{\varepsilon}^S + \boldsymbol{\varepsilon}^D = 0$ in Ω^{r} from (46). Hence, the restriction of $\boldsymbol{X}^S$ to Ω^{r} is kinematically compatible, which means that it is equal to the symmetric part of the gradient of some displacement vector field on Ω^{r}. It appears that the restriction of $\boldsymbol{X}^S$ to Ω^{r} solve a Neumann boundary elasticity problem on this domain when occupied by the reference material $\boldsymbol{C}_0$ with free body force and prescribed stress vector $(\boldsymbol{C}_0 : \boldsymbol{X}^S) \cdot \boldsymbol{n}$ at the boundary $\partial\Omega^{\mathrm{r}}$ of Ω^{r}, where $\boldsymbol{n}$ is the outer normal to $\partial\Omega^{\mathrm{r}}$. In particular, if Ω^{r} is regular as defined below then the above described Neumann boundary elasticity problem has a unique solution. This means that the restriction of $\boldsymbol{X}^S$ to Ω^{r} appears as an unambiguously defined extension of its values on $\Omega \setminus \Omega^{\mathrm{r}}$.

Characterizing $\boldsymbol{X}^D$ in the pores. Note that, since $\boldsymbol{\sigma}$ is null in Ω^{p}, then $\boldsymbol{C}_0 : \boldsymbol{X}^D$ is divergence-free in Ω^{p}. By definition of $\boldsymbol{X}^D$, there exists a unique Ω-periodic displacement field in $H^1(\Omega)^d$, $\boldsymbol{u}$, with $\langle \boldsymbol{u} \rangle_\Omega = 0$ such that the symmetric part of its gradient is equal to $\boldsymbol{X}^D$. It appears that the restriction of $\boldsymbol{u}$ to Ω^{p} solves a Dirichlet-type elasticity problem with free body force on this domain when occupied by the reference material $\boldsymbol{C}_0$. In particular, if Ω^{p} is regular as defined below then the above described Dirichlet boundary elasticity problem has a unique solution. This means that the restriction of $\boldsymbol{X}^D$ to Ω^{p} appears as an unambiguously defined extension of its values on $\Omega \setminus \Omega^{\mathrm{p}}$.

4.2. Regularity requirements

In the present section, we state the mathematical restrictions that apply to $\boldsymbol{C}$, Ω^{r} and Ω^{p} for the existence and uniqueness of a solution of the homogenization problem (47) and for the AEM scheme to be convergent. For this purpose, it is useful to introduce the following definitions which derive from the remarkable properties of $\boldsymbol{X}^S$ and $\boldsymbol{X}^D$ described in the previous section.

Definition 1 (Subspace $\boldsymbol{S}^r$)**.** *$\boldsymbol{S}^r$ is the subspace of stress fields $\boldsymbol{\sigma}$ in $\boldsymbol{S}$ such that $\boldsymbol{C}_0^{-1} : \boldsymbol{\sigma}$ is kinematically compatible in Ω^{r} (equal to the symmetric part of the gradient of some displacement vector field on Ω^{r}). We say that such stress fields are $\boldsymbol{C}_0$-extended in the rigid inclusions.*

Owing to the theorem of J.-J. Moreau on the compatibility conditions [23], it is seen that $\boldsymbol{S}^r$ is a closed subset of $\boldsymbol{S}$.

Definition 2 (Subspace $\boldsymbol{D}^p$)**.** *$\boldsymbol{D}^p$ is the closed subspace of strain fields $\boldsymbol{e}$ in $\boldsymbol{D}$ such that $\boldsymbol{C}_0 : \boldsymbol{e}$ is divergence-free in Ω^{p}. We say that such strain fields are $\boldsymbol{C}_0$-extended in the pores.*

Definition 3 (Subspace $\boldsymbol{L}^2_{\mathrm{ext}}(\Omega)$)**.** *$\boldsymbol{L}^2_{\mathrm{ext}}(\Omega)$ is the closed subset of $\boldsymbol{e}$ in $\boldsymbol{L}^2_{\mathrm{sym}}(\Omega)$ such that: $\boldsymbol{e}^D \in \boldsymbol{D}^p$ and $\boldsymbol{C}_0 : \boldsymbol{e}^S \in \boldsymbol{S}^r$. It is seen from the previous section that any residual field $\boldsymbol{X}$ corresponding to a pair of strain-stress fields complying to the constitutive equations (46) is in $\boldsymbol{L}^2_{\mathrm{ext}}(\Omega)$. Moreover, under the S- and D-regularity conditions defined below, there exists a constant $c > 1$, independent of $\boldsymbol{X}$, such that:*

$$\int_\Omega \boldsymbol{X} : \boldsymbol{C}_0 : \boldsymbol{X} = \int_\Omega \boldsymbol{X}^S : \boldsymbol{C}_0 : \boldsymbol{X}^S + \int_\Omega \boldsymbol{X}^D : \boldsymbol{C}_0 : \boldsymbol{X}^D \leq c \left(\int_{\Omega\setminus\Omega^{\mathrm{r}}} \boldsymbol{X}^S : \boldsymbol{C}_0 : \boldsymbol{X}^S + \int_{\Omega\setminus\Omega^{\mathrm{p}}} \boldsymbol{X}^D : \boldsymbol{C}_0 : \boldsymbol{X}^D \right) \tag{51}$$

Definition 4 (S-regularity)**.** *The domain Ω^{r} occupied by the rigid inclusions is S-regular if there exists a constant $c > 0$ such that:*

$$\int_\Omega \boldsymbol{e} : \boldsymbol{C}_0 : \boldsymbol{e} \leq c \int_{\Omega\setminus\Omega^{\mathrm{r}}} \boldsymbol{e} : \boldsymbol{C}_0 : \boldsymbol{e}, \tag{52}$$

for all $\boldsymbol{e} \in \boldsymbol{L}^2_{\mathrm{sym}}(\Omega)$ such that $\boldsymbol{C}_0 : \boldsymbol{e} \in \boldsymbol{S}^r$.

Definition 5 (D-regularity)**.** *The domain Ω^{p} occupied by the pores is D-regular if there exists a constant $c > 0$ such that:*

$$\int_\Omega \boldsymbol{e} : \boldsymbol{C}_0 : \boldsymbol{e} \leq c \int_{\Omega\setminus\Omega^{\mathrm{p}}} \boldsymbol{e} : \boldsymbol{C}_0 : \boldsymbol{e}, \tag{53}$$

for all $\boldsymbol{e} \in \boldsymbol{D}^p$.

It is shown in Appendix C (resp. Appendix D) that if Ω^{r} (resp. Ω^{p}) is the union of Ω-periodic non-intersecting Lipschitz domains [1] (which guarantees that the microstructure is mechanically stable and deformable), then it is S-regular (resp. D-regular).

In the remainder of this paper, we assume that: (i) $\boldsymbol{C}$ is uniformly coercive (in the sense of Equation (4) over Ω^{m}, (ii) Ω^{r} is S-regular and (iii) Ω^{p} is D-regular.

In [24], the author considered porous media in which he extended the displacement field in the pores by imposing the displacement at the pores boundaries and solving inside the pores a homogeneous Dirichlet-type elasticity problem with stiffness equal to the identity. This regularization actually corresponds to our D-regularity where the reference material is set to identity. So, D-regularity and S-regularity can be seen as natural extensions of the regularization proposed in [24].

[1] A Lipschitz domain is a non-empty connected open set with Lipschitz boundary

4.3. The proposed scheme

We now state the AEM scheme in the case of regular pores and regular rigid inclusions embedded in a heterogeneous matrix. The algorithm is started with a chosen pair of strain-stress fields in the unit-cell $(\boldsymbol{\varepsilon}^0, \boldsymbol{\sigma}^0)$ verifying (46) and its corresponding residual $\boldsymbol{X}^0$ is computed with formula (49). For $n \geq 0$, if $\boldsymbol{X}^n = 0$ then the pair $(\boldsymbol{\varepsilon}^n, \boldsymbol{\sigma}^n)$ is a solution of the homogenization problem, and the iteration is stopped. Otherwise, compute $\boldsymbol{X}^{n+1}$, $\boldsymbol{\varepsilon}^{n+1}$ and $\boldsymbol{\sigma}^{n+1}$ as follows:

$$\boldsymbol{Z}^n = \boldsymbol{\alpha} : \boldsymbol{X}^n + \boldsymbol{\Gamma}^0 * [(\boldsymbol{C}^D - \boldsymbol{C}^S) : \boldsymbol{X}^n] \tag{54}$$

$$\lambda^n = \frac{\langle \boldsymbol{X}^n : \boldsymbol{C}_0 : \boldsymbol{Z}^n \rangle_\Omega}{\langle \boldsymbol{Z}^n : \boldsymbol{C}_0 : \boldsymbol{Z}^n \rangle_\Omega} \tag{55}$$

$$\boldsymbol{X}^{n+1} = \boldsymbol{X}^n - \lambda^n \boldsymbol{Z}^n = \boldsymbol{X}^0 - \sum_{k=0}^{n} \lambda^k \boldsymbol{Z}^k, \tag{56}$$

$$\boldsymbol{\varepsilon}^{n+1} = \boldsymbol{\varepsilon}^n + \lambda^n \boldsymbol{\alpha} : \boldsymbol{X}^n = \boldsymbol{\varepsilon}^0 + \boldsymbol{\alpha} : \sum_{k=0}^{n} \lambda^k \boldsymbol{X}^k, \tag{57}$$

$$\boldsymbol{\sigma}^{n+1} = \boldsymbol{\sigma}^n + \lambda^n \boldsymbol{C}^D : \boldsymbol{X}^n = \boldsymbol{\sigma}^0 + \boldsymbol{C}^D : \sum_{k=0}^{n} \lambda^k \boldsymbol{X}^k. \tag{58}$$

Assuming that the pair $(\boldsymbol{\varepsilon}^n, \boldsymbol{\sigma}^n)$ verifies the constitutive equations (46) and $\boldsymbol{X}^n$ being its corresponding residual (which is in $\boldsymbol{L}^2_{\text{ext}}(\Omega)$ according to Section 4.1 and Definition 3), let us check that the pair $(\boldsymbol{\varepsilon}^{n+1}, \boldsymbol{\sigma}^{n+1})$ defined above verifies the constitutive equations (46) and that its corresponding residual $\boldsymbol{X}^{n+1}$ (also in $\boldsymbol{L}^2_{\text{ext}}(\Omega)$) is actually given by (56). Indeed, from the definition of $\boldsymbol{\alpha}$ and $\boldsymbol{C}^D$, we see that: $\boldsymbol{\varepsilon}^{n+1}$ is null in Ω^{r}, $\boldsymbol{\sigma}^{n+1}$ is null in Ω^{p} and $\boldsymbol{\sigma}^{n+1} = \boldsymbol{C} : \boldsymbol{\varepsilon}^{n+1}$ in Ω^{m}. Finally, inserting $(\boldsymbol{\varepsilon}^{n+1}, \boldsymbol{\sigma}^{n+1})$ in (49) leads to (56).

It results from Section 4.1 that $(\boldsymbol{\varepsilon}^n, \boldsymbol{\sigma}^n)$ is a solution to the homogenization problem (47) if, and only if $\boldsymbol{X}^n = 0$. It is therefore natural to stop the iterations when $\boldsymbol{X}^n$ is "small enough", as discussed in Section 7.2.

5. Proof of convergence

5.1. Statement of the convergence result and outline of the proof

Under the regularity conditions stated in Section 4.2, the iterative scheme described in Section 4.3 is linearly convergent. Besides, the sequence of pairs $(\boldsymbol{\varepsilon}^n, \boldsymbol{\sigma}^n)$ converges to a solution of the extended homogenization problem (47). This problem has a unique solution up to a pair $(\boldsymbol{e}, \boldsymbol{\sigma}) \in \boldsymbol{D} \times \boldsymbol{S}$ with $(\boldsymbol{e}, \boldsymbol{\sigma}) = (0, 0)$ in Ω^{m}. Finally, these results hold for any choices of initial pair $(\boldsymbol{\varepsilon}^0, \boldsymbol{\sigma}^0)$ verifying (46) and reference medium $\boldsymbol{C}_0$.

It is emphasized that the iterations are **unconditionally convergent**, regardless of the actual choice of the reference medium $\boldsymbol{C}_0$.

Proof. Using simple algebra:

$$\|\boldsymbol{X}^{n+1}\|^2_{\boldsymbol{C}_0} = \|\boldsymbol{X}^n\|^2_{\boldsymbol{C}_0} - \frac{\langle \boldsymbol{X}^n : \boldsymbol{C}_0 : \boldsymbol{Z}^n \rangle^2_\Omega}{\langle \boldsymbol{Z}^n : \boldsymbol{C}_0 : \boldsymbol{Z}^n \rangle_\Omega} \tag{59}$$

It will be shown in Section 5.2 that there exist two real constants $0 < a < 1$ and $0 < b$ such that for any $n \geq 0$:

$$\|\boldsymbol{X}^{n+1}\|_{\boldsymbol{C}_0} \leq a \|\boldsymbol{X}^n\|_{\boldsymbol{C}_0} \text{ and } 0 < \lambda^n \leq b, \tag{60}$$

from which it results that $\|\boldsymbol{X}^n\|_{\boldsymbol{C}_0} \leq a^n \|\boldsymbol{X}^0\|_{\boldsymbol{C}_0}$ and hence the sequence $\|\boldsymbol{X}^n\|_{\boldsymbol{C}_0}$ converges to zero as n goes to infinity.

Moreover, the λ^k being uniformly bounded, the series $\sum_{k=0}^{n} \lambda^k \boldsymbol{X}^k$ in (57) and (58) converges normally. Hence, $(\boldsymbol{\varepsilon}^n, \boldsymbol{\sigma}^n)$ converge in $\boldsymbol{L}^2_{\text{sym}}(\Omega) \times \boldsymbol{L}^2_{\text{sym}}(\Omega)$ to a limit $(\boldsymbol{\varepsilon}^\infty, \boldsymbol{\sigma}^\infty)$. Owing to the continuity in $\boldsymbol{L}^2_{\text{sym}}(\Omega)$ of the linear map $(\boldsymbol{\varepsilon}, \boldsymbol{\sigma}) \longmapsto \boldsymbol{X}$ we find that the residual $\boldsymbol{X}^\infty$ associated to $(\boldsymbol{\varepsilon}^\infty, \boldsymbol{\sigma}^\infty)$ is null, which ensures that $(\boldsymbol{\varepsilon}^\infty, \boldsymbol{\sigma}^\infty)$ is a solution to the homogenization problem (47).

Finally, we show that this solution is unique up to a pair $(\boldsymbol{e}, \boldsymbol{\sigma}) \in \boldsymbol{D} \times \boldsymbol{S}$ with $(\boldsymbol{e}, \boldsymbol{\sigma}) = (0, 0)$ in Ω^{m}. Indeed, let $(\Delta\boldsymbol{e}_E, \Delta\boldsymbol{\sigma}_E)$ represent the difference between two solutions of the above homogenization problem. Then, $(\Delta\boldsymbol{e}_E, \Delta\boldsymbol{\sigma}_E) \in \boldsymbol{D} \times \boldsymbol{S}$ complies with (46). We have, $< \Delta\boldsymbol{\sigma}_E : \Delta\boldsymbol{e}_E >_\Omega = 0$ and hence $< \Delta\boldsymbol{e}_E : \boldsymbol{C} : \Delta\boldsymbol{e}_E >_{\Omega^{\text{m}}} = 0$. Finally, using (4) in the matrix domain Ω^{m} leads to $(\Delta\boldsymbol{e}_E, \Delta\boldsymbol{\sigma}_E) = (0, 0)$ in Ω^{m}.

5.2. Detailed proof of the convergence result

The proof of the convergence result stated in the previous section will be complete when (60) is proved. To this end, it is useful to introduce the linear map $\boldsymbol{X} \longmapsto \boldsymbol{Z}(\boldsymbol{X})$ which maps $\boldsymbol{X} \in \boldsymbol{L}^2_{\rm sym}(\Omega)$ to its AEM-scheme optimization direction $\boldsymbol{Z}(\boldsymbol{X})$ given by:

$$\boldsymbol{Z}(\boldsymbol{X}) = \boldsymbol{\alpha} : \boldsymbol{X} + \boldsymbol{\Gamma}^0 * [(\boldsymbol{C}^D - \boldsymbol{C}^S) : \boldsymbol{X}]. \tag{61}$$

We also define the functional $\lambda(\boldsymbol{X})$ corresponding to the step-size in the $\boldsymbol{Z}(\boldsymbol{X})$ direction. We will respectively write $\boldsymbol{Z}$ and λ instead of $\boldsymbol{Z}(\boldsymbol{X})$ and $\lambda(\boldsymbol{X})$ for the sake and simplicity. If $\boldsymbol{Z} \neq 0$, then λ is given by:

$$\lambda = \frac{\langle \boldsymbol{X} : \boldsymbol{C}_0 : \boldsymbol{Z} \rangle_\Omega}{\langle \boldsymbol{Z} : \boldsymbol{C}_0 : \boldsymbol{Z} \rangle_\Omega} \tag{62}$$

Recalling that $\boldsymbol{X}^n$ is the residual of the strain-stress pair $(\boldsymbol{\varepsilon}^n, \boldsymbol{\sigma}^n)$ complying to the constitutive equations (46), it is seen that $\boldsymbol{X}^n$ is actually in $\boldsymbol{L}^2_{\rm ext}(\Omega)$ according to Section 4.1 and Definition 3. In order to prove (60), we will show that there exist two real constants $0 < a < 1$ and $0 < b$ such that for any $\boldsymbol{X} \neq 0$ in $\boldsymbol{L}^2_{\rm ext}(\Omega)$, we have:

$$\|\boldsymbol{X} - \lambda \boldsymbol{Z}\|_{\boldsymbol{C}_0} \leq a \|\boldsymbol{X}\|_{\boldsymbol{C}_0} \;\text{ and }\; 0 < \lambda \leq b. \tag{63}$$

The proof proceeds in four steps.

First step. The linear map $\boldsymbol{X} \longmapsto \boldsymbol{Z}(\boldsymbol{X})$ defined by (61) is continuous in $\boldsymbol{L}^2_{\rm sym}(\Omega)$ due to the continuity of the Green operator $\boldsymbol{\Gamma}^0$ and the fact that $\boldsymbol{C}^S(\boldsymbol{y})$ and $\boldsymbol{C}^D(\boldsymbol{y})$ are uniformly bounded by $2\boldsymbol{C}_0$. Indeed, since $\boldsymbol{C}_0^{-1} : \boldsymbol{C}^S = \boldsymbol{\alpha}$ and $\boldsymbol{C}_0^{-1} : \boldsymbol{C}^D = 2\boldsymbol{I} - \boldsymbol{\alpha}$, one can rewrite $\boldsymbol{Z}$ as:

$$\boldsymbol{Z} = \boldsymbol{\alpha} : \boldsymbol{X} + (\boldsymbol{C}_0^{-1} : (\boldsymbol{C}^D - \boldsymbol{C}^S) : \boldsymbol{X})^D = (\boldsymbol{C}_0^{-1} : \boldsymbol{C}^S : \boldsymbol{X})^S + (\boldsymbol{C}_0^{-1} : \boldsymbol{C}^D : \boldsymbol{X})^D = (\boldsymbol{\alpha} : \boldsymbol{X})^S + ((2\boldsymbol{I} - \boldsymbol{\alpha}) : \boldsymbol{X})^D \tag{64}$$

Using the above orthogonal decomposition, we have:

$$\forall \boldsymbol{X} \in \boldsymbol{L}^2_{\rm sym}(\Omega), \quad \langle \boldsymbol{Z} : \boldsymbol{C}_0 : \boldsymbol{Z} \rangle_\Omega \;=\; \|(\boldsymbol{C}_0^{-1} : \boldsymbol{C}^S : \boldsymbol{X})^S\|^2_{\boldsymbol{C}_0} + \|(\boldsymbol{C}_0^{-1} : \boldsymbol{C}^D : \boldsymbol{X})^D\|^2_{\boldsymbol{C}_0} \tag{65}$$

Hence, recalling that the $S-$ and D-projections are contracting linear operators, we have:

$$\forall \boldsymbol{X} \in \boldsymbol{L}^2_{\rm sym}(\Omega), \quad \langle \boldsymbol{Z} : \boldsymbol{C}_0 : \boldsymbol{Z} \rangle_\Omega \;\leq\; \langle \boldsymbol{X} : \boldsymbol{C}^S : \boldsymbol{C}_0^{-1} : \boldsymbol{C}^S : \boldsymbol{X} \rangle_\Omega + \langle \boldsymbol{X} : \boldsymbol{C}^D : \boldsymbol{C}_0^{-1} : \boldsymbol{C}^D : \boldsymbol{X} \rangle_\Omega \;\leq\; 8 \langle \boldsymbol{X} : \boldsymbol{C}_0 : \boldsymbol{X} \rangle_\Omega \tag{66}$$

where the last inequality is proved in Appendix B. It should be emphasized that (66) still holds true even in the absence of the uniform coercivity condition (9).

Second step: the key equation. We have the following key equation:

$$\forall \boldsymbol{X} \in \boldsymbol{L}^2_{\rm sym}(\Omega), \quad \langle \boldsymbol{X} : \boldsymbol{C}_0 : \boldsymbol{Z} \rangle_\Omega = \langle \boldsymbol{X}^S : \boldsymbol{C}^S : \boldsymbol{X}^S \rangle_\Omega + \langle \boldsymbol{X}^D : \boldsymbol{C}^D : \boldsymbol{X}^D \rangle_\Omega \tag{67}$$

Using (64), we have:

$$\begin{aligned}
\langle \boldsymbol{X} : \boldsymbol{C}_0 : \boldsymbol{Z} \rangle_\Omega &= \langle \boldsymbol{X} : \boldsymbol{C}_0 : (\boldsymbol{C}_0^{-1} : \boldsymbol{C}^S : \boldsymbol{X})^S \rangle_\Omega + \langle \boldsymbol{X} : \boldsymbol{C}_0 : (\boldsymbol{C}_0^{-1} : \boldsymbol{C}^D : \boldsymbol{X})^D \rangle_\Omega \\
&= \langle \boldsymbol{X}^S : \boldsymbol{C}_0 : \boldsymbol{C}_0^{-1} : \boldsymbol{C}^S : \boldsymbol{X} \rangle_\Omega + \langle \boldsymbol{X}^D : \boldsymbol{C}_0 : \boldsymbol{C}_0^{-1} : \boldsymbol{C}^D : \boldsymbol{X} \rangle_\Omega \\
&= \langle \boldsymbol{X}^S : \boldsymbol{C}^S : \boldsymbol{X} \rangle_\Omega + \langle \boldsymbol{X}^D : \boldsymbol{C}^D : \boldsymbol{X} \rangle_\Omega \\
&= \langle \boldsymbol{X}^S : \boldsymbol{C}^S : \boldsymbol{X}^S \rangle_\Omega + \langle \boldsymbol{X}^D : \boldsymbol{C}^D : \boldsymbol{X}^D \rangle_\Omega + \langle \boldsymbol{X}^S : \boldsymbol{C}^S : \boldsymbol{X}^D \rangle_\Omega + \langle \boldsymbol{X}^D : \boldsymbol{C}^D : \boldsymbol{X}^S \rangle_\Omega \\
&= \langle \boldsymbol{X}^S : \boldsymbol{C}^S : \boldsymbol{X}^S \rangle_\Omega + \langle \boldsymbol{X}^D : \boldsymbol{C}^D : \boldsymbol{X}^D \rangle_\Omega + \langle \boldsymbol{X}^D : (\boldsymbol{C}^D + \boldsymbol{C}^S) : \boldsymbol{X}^S \rangle_\Omega \\
&= \langle \boldsymbol{X}^S : \boldsymbol{C}^S : \boldsymbol{X}^S \rangle_\Omega + \langle \boldsymbol{X}^D : \boldsymbol{C}^D : \boldsymbol{X}^D \rangle_\Omega + \langle \boldsymbol{X}^D : 2\boldsymbol{C}_0 : \boldsymbol{X}^S \rangle_\Omega \\
&= \langle \boldsymbol{X}^S : \boldsymbol{C}^S : \boldsymbol{X}^S \rangle_\Omega + \langle \boldsymbol{X}^D : \boldsymbol{C}^D : \boldsymbol{X}^D \rangle_\Omega,
\end{aligned}$$

where properties (19) and (38) have been used. $\boldsymbol{C}^S$ and $\boldsymbol{C}^D$ being positive, the key equation (67) shows that $\boldsymbol{X} \longmapsto \langle \boldsymbol{X} : \boldsymbol{C}_0 : \boldsymbol{Z} \rangle_\Omega$ is a positive quadratic form on $\boldsymbol{L}^2_{\rm sym}(\Omega)$.

In the next step, we will establish (63) under the following assumption: there exists a $\boldsymbol{C}_0$-dependent constant $0 < \kappa_0 < 1$ such that:

$$\forall \boldsymbol{X} \in \boldsymbol{L}^2_{\rm ext}(\Omega), \quad \langle \boldsymbol{X} : \boldsymbol{C}_0 : \boldsymbol{Z} \rangle_\Omega \geq \kappa_0 \langle \boldsymbol{X} : \boldsymbol{C}_0 : \boldsymbol{X} \rangle_\Omega \tag{68}$$

Third step. From the Cauchy-Schwartz inequality and (68), we obtain:

$$\forall \boldsymbol{X} \in \boldsymbol{L}^2_{\text{ext}}(\Omega), \quad \sqrt{\langle \boldsymbol{Z} : \boldsymbol{C}_0 : \boldsymbol{Z} \rangle_\Omega} \sqrt{\langle \boldsymbol{X} : \boldsymbol{C}_0 : \boldsymbol{X} \rangle_\Omega} \geq \langle \boldsymbol{X} : \boldsymbol{C}_0 : \boldsymbol{Z} \rangle_\Omega \geq \kappa_0 \langle \boldsymbol{X} : \boldsymbol{C}_0 : \boldsymbol{X} \rangle_\Omega. \tag{69}$$

If $\boldsymbol{X} \neq 0$, we get

$$\sqrt{\langle \boldsymbol{Z} : \boldsymbol{C}_0 : \boldsymbol{Z} \rangle_\Omega} \geq \kappa_0 \sqrt{\langle \boldsymbol{X} : \boldsymbol{C}_0 : \boldsymbol{X} \rangle_\Omega}. \tag{70}$$

If $\boldsymbol{X} = 0$, we have trivially $\boldsymbol{Z} = 0$ (see (61)) and the above inequality also holds. Conversely, (70) implies that $\boldsymbol{Z} \neq 0$ for any $\boldsymbol{X} \neq 0$ in $\boldsymbol{L}^2_{\text{ext}}(\Omega)$, hence λ is well-defined by (62). Now, inserting (70) in the left-hand part of (69), we obtain:

$$\forall \boldsymbol{X} \in \boldsymbol{L}^2_{\text{ext}}(\Omega), \quad 8\kappa_0^{-1} \langle \boldsymbol{X} : \boldsymbol{C}_0 : \boldsymbol{X} \rangle_\Omega \geq \kappa_0^{-1} \langle \boldsymbol{Z} : \boldsymbol{C}_0 : \boldsymbol{Z} \rangle_\Omega \geq \langle \boldsymbol{X} : \boldsymbol{C}_0 : \boldsymbol{Z} \rangle_\Omega \geq \kappa_0 \langle \boldsymbol{X} : \boldsymbol{C}_0 : \boldsymbol{X} \rangle_\Omega. \tag{71}$$

This means that the functionals $\boldsymbol{X} \longmapsto \sqrt{\langle \boldsymbol{X} : \boldsymbol{C}_0 : \boldsymbol{Z} \rangle_\Omega}$ and $\boldsymbol{X} \longmapsto \sqrt{\langle \boldsymbol{Z} : \boldsymbol{C}_0 : \boldsymbol{Z} \rangle_\Omega}$ are actually norms over $\boldsymbol{L}^2_{\text{ext}}(\Omega)$ and these norms are equivalent to the $\boldsymbol{C}_0$-norm. Moreover, for any $\boldsymbol{X} \neq 0$ in $\boldsymbol{L}^2_{\text{ext}}(\Omega)$ the corresponding λ is uniformly bounded:

$$0 < \frac{\kappa_0}{8} \leq \lambda = \frac{\langle \boldsymbol{X} : \boldsymbol{C}_0 : \boldsymbol{Z} \rangle_\Omega}{\langle \boldsymbol{Z} : \boldsymbol{C}_0 : \boldsymbol{Z} \rangle_\Omega} \leq \kappa_0^{-1}, \tag{72}$$

and, combining (66), (69) and (71), we obtain:

$$1 \geq \frac{\langle \boldsymbol{X} : \boldsymbol{C}_0 : \boldsymbol{Z} \rangle^2_\Omega}{\langle \boldsymbol{Z} : \boldsymbol{C}_0 : \boldsymbol{Z} \rangle_\Omega \langle \boldsymbol{X} : \boldsymbol{C}_0 : \boldsymbol{X} \rangle_\Omega} \geq \frac{\kappa_0^2}{8}, \tag{73}$$

Finally, using the following equation:

$$\|\boldsymbol{X} - \lambda \boldsymbol{Z}\|^2_{\boldsymbol{C}_0} = \|\boldsymbol{X}\|^2_{\boldsymbol{C}_0} - \frac{\langle \boldsymbol{X} : \boldsymbol{C}_0 : \boldsymbol{Z} \rangle^2_\Omega}{\langle \boldsymbol{Z} : \boldsymbol{C}_0 : \boldsymbol{Z} \rangle_\Omega}, \tag{74}$$

we see that (63) holds for a equal to $\sqrt{1 - \frac{\kappa_0^2}{8}}$ and b equal to κ_0^{-1}.

It should be pointed out that the minimum possible values for a and b in (63), respectively noted a_0^- and b_0^- with $0 < a_0^- \leq \sqrt{1 - \frac{\kappa_0^2}{8}} < 1$ and $0 < b_0^- \leq \kappa_0^{-1}$, are such that:

$$\sqrt{1 - (a_0^-)^2} = \inf \frac{\langle \boldsymbol{X} : \boldsymbol{C}_0 : \boldsymbol{Z} \rangle^2_\Omega}{\langle \boldsymbol{Z} : \boldsymbol{C}_0 : \boldsymbol{Z} \rangle_\Omega \langle \boldsymbol{X} : \boldsymbol{C}_0 : \boldsymbol{X} \rangle_\Omega}, \tag{75}$$

and

$$b_0^- = \sup \frac{\langle \boldsymbol{X} : \boldsymbol{C}_0 : \boldsymbol{Z} \rangle_\Omega}{\langle \boldsymbol{Z} : \boldsymbol{C}_0 : \boldsymbol{Z} \rangle_\Omega}, \tag{76}$$

where the above infinimum and supremum are taken over all $\boldsymbol{X} \neq 0$ in $\boldsymbol{L}^2_{\text{ext}}(\Omega)$.

Clearly, a_0^- and b_0^- are $\boldsymbol{C}_0$-dependent. And hence, the rate of convergence of the AEM-scheme is $\boldsymbol{C}_0$-dependent.

Fourth step. It is important to note that (63) holds true, and hence the AEM scheme linearly converges, for any periodic elasticity tensor fields satisfying (68). Indeed, we have not yet used any of the regularity requirements stated in Section 4.2. We will prove now that these requirements are sufficient to satisfy (68) for any choice of the reference material $\boldsymbol{C}_0$.

Owing to the regularity assumptions on $\boldsymbol{C}$ in the heterogeneous matrix, we know that (39)–(41) holds in Ω^{m}. Further remembering that $\boldsymbol{C}^S = 0$ in the rigid inclusions and $\boldsymbol{C}^D = 0$ in the pores, we get:

$$\int_\Omega \boldsymbol{X} : \boldsymbol{C}_0 : \boldsymbol{Z} \geq \int_{\Omega \setminus \Omega^{\text{r}}} \boldsymbol{X}^S : \boldsymbol{C}^{S-} : \boldsymbol{X}^S + \int_{\Omega \setminus \Omega^{\text{p}}} \boldsymbol{X}^D : \boldsymbol{C}^{D-} : \boldsymbol{X}^D \geq d \left(\int_{\Omega \setminus \Omega^{\text{r}}} \boldsymbol{X}^S : \boldsymbol{C}_0 : \boldsymbol{X}^S + \int_{\Omega \setminus \Omega^{\text{p}}} \boldsymbol{X}^D : \boldsymbol{C}_0 : \boldsymbol{X}^D \right) \tag{77}$$

where the constant $0 < d \leq 1$ is given by:

$$d = \min \left\{ \frac{2}{1 + \mu^+}, \frac{2\mu^-}{1 + \mu^-} \right\}. \tag{78}$$

Finally, for any $\boldsymbol{X}$ is in $\boldsymbol{L}^2_{\text{ext}}(\Omega)$, one can combine (51) with (77) to obtain (68) with

$$\kappa_0 = \frac{d}{c} \tag{79}$$

where $c > 1$ is the constant in (51) and the bounds:

$$a_0^- \leq \sqrt{1 - \frac{d^2}{8c^2}} < 1, \quad b_0^- \leq \frac{c}{d}. \tag{80}$$

6. Characterization of the limit of the AEM iterations

We have just shown that the AEM iterations converge to a solution of the homogenization problem. Indeed, it is recalled that the mechanical fields are unique in the matrix only. From the point of view of homogenization, this is of no importance, since the homogenized stiffness only depends on the mechanical fields *in the matrix*. However, it is interesting to determine which of these solutions is selected by the AEM iterations, if only to understand how the iterative scheme works. We will show that for a natural choice of initialization of these iterations, their limit is the unique $\boldsymbol{C}_0$-extended solution of the Lippmann–Schwinger equation.

6.1. The zero-initialization of the AEM iterations

The AEM scheme imposes no requirement on the initial strain field $\boldsymbol{\varepsilon}^0$. In particular, there is no need for $\boldsymbol{\varepsilon}^0$ to be compatible (i.e. the sum of $\boldsymbol{E}$ and a strain field in $\boldsymbol{D}$). Therefore, one could take advantage of this by selecting an initial strain different from the usual initialization $\boldsymbol{\varepsilon}^0 = \boldsymbol{E}$, which is not suitable for composites containing infinitely rigid inclusions.

Actually, the simplest initialization in the AEM scheme is to set to zero both initial strain and initial stress:

$$\boldsymbol{\varepsilon}^0(\boldsymbol{y}) = 0, \quad \boldsymbol{\sigma}^0(\boldsymbol{y}) = 0, \quad \boldsymbol{X}^0(\boldsymbol{y}) = \boldsymbol{E}. \tag{81}$$

With this zero-initialization, the AEM scheme converges to a solution to the homogenization problem which writes:

$$\boldsymbol{\varepsilon}_E = \boldsymbol{\alpha}(\boldsymbol{y}) : \boldsymbol{\varepsilon}^*_E(\boldsymbol{y}), \quad \boldsymbol{\sigma}_E = \boldsymbol{C}^D(\boldsymbol{y}) : \boldsymbol{\varepsilon}^*_E(\boldsymbol{y}), \tag{82}$$

where the auxiliary strain field $\boldsymbol{\varepsilon}^*_E$ is given by:

$$\boldsymbol{\varepsilon}^*_E(\boldsymbol{y}) = \sum_{k\geq 0} \lambda^k \boldsymbol{X}^k(\boldsymbol{y}), \tag{83}$$

see Eqs. (57) and (58) with $\boldsymbol{\varepsilon}^0 = 0$ and $\boldsymbol{\sigma}^0 = 0$. Moreover, inserting equation $\boldsymbol{C}^D = 2\boldsymbol{C}_0 - \boldsymbol{C}^S = 2\boldsymbol{C}_0 - \boldsymbol{C}_0 : \boldsymbol{\alpha}$ in (82), and using simple algebra leads to the following expression of $\boldsymbol{\varepsilon}^*_E$:

$$\boldsymbol{\varepsilon}^*_E = \frac{1}{2}\left((\boldsymbol{C}_0)^{-1} : \boldsymbol{\sigma}_E + \boldsymbol{\varepsilon}_E\right) \tag{84}$$

which can be decomposed as $\boldsymbol{\varepsilon}^*_E = \boldsymbol{\varepsilon}^{*S}_E + \boldsymbol{\varepsilon}^{*D}_E$ with:

$$\boldsymbol{\varepsilon}^{*S}_E = \frac{1}{2}\left((\boldsymbol{C}_0)^{-1} : \boldsymbol{\sigma}_E + \boldsymbol{E}\right), \quad \boldsymbol{\varepsilon}^{*D}_E = \frac{1}{2}\boldsymbol{\varepsilon}^D_E. \tag{85}$$

Notice that the auxiliary strain $\boldsymbol{\varepsilon}^*_E$ is related to the so-called P-polarization $\boldsymbol{P}_E$ by the following equation (see [17]):

$$\boldsymbol{P}_E = \boldsymbol{\sigma}_E + \boldsymbol{C}_0 : \boldsymbol{\varepsilon}_E = 2\boldsymbol{C}_0 : \boldsymbol{\varepsilon}^*_E \tag{86}$$

6.2. Characterization of the solution defined by the zero-initialisation

With the previous choice of initialization, we select a solution, which we show to be the only one that is $\boldsymbol{C}_0$-extended. Indeed, $\boldsymbol{\varepsilon}_E^*$ is actually in $\boldsymbol{L}^2_{\text{ext}}(\Omega)$ as the limit of linear combination of elements of $\boldsymbol{L}^2_{\text{ext}}(\Omega)$. Therefore, by definition of $\boldsymbol{L}^2_{\text{ext}}(\Omega)$, we can write:

$$\boldsymbol{C}_0 : \boldsymbol{\varepsilon}_E^{*S} = \frac{1}{2}\left(\boldsymbol{\sigma}_E + \boldsymbol{C}_0 : \boldsymbol{E}\right) \in \boldsymbol{S}^r, \quad \boldsymbol{\varepsilon}_E^{*D} = \frac{1}{2}\boldsymbol{\varepsilon}_E^D \in \boldsymbol{D}^p, \tag{87}$$

and $\boldsymbol{C}_0 : \boldsymbol{E}$ being obviously in $\boldsymbol{S}^r$, the above properties imply:

$$\boldsymbol{\sigma}_E \in \boldsymbol{S}^r, \quad \boldsymbol{\varepsilon}_E^D \in \boldsymbol{D}^p, \tag{88}$$

which means that $\boldsymbol{\sigma}_E$ is $\boldsymbol{C}_0$-extended in the rigid inclusions and $\boldsymbol{\varepsilon}_E^D$ is $\boldsymbol{C}_0$-extended in the pores.

6.3. The modified Lippmann–Schwinger equation

It is remarkable to observe that the new variable is the only solution to a problem that resembles a homogenization problem, for a material of finite fictitious stiffness (no pores, no rigid inclusions). In this subsection, we set out the modified Lippmann–Schwinger whose unique $\boldsymbol{C}_0$-extended solution is the auxiliary strain field $\boldsymbol{\varepsilon}_E^*$.

Recall that the solution (82) is such that its residual (49) is null. Hence, $\boldsymbol{\varepsilon}_E^*$ is a solution to the following modified Lippmann–Schwinger equation:

$$\boldsymbol{Z}(\boldsymbol{\varepsilon}^*) = \boldsymbol{E}, \tag{89}$$

where the $\boldsymbol{Z}$-operator is given by (61) and the residual writes:

$$\boldsymbol{X}(\boldsymbol{\varepsilon}^*) = \boldsymbol{E} - \boldsymbol{Z}(\boldsymbol{\varepsilon}^*). \tag{90}$$

Actually, $\boldsymbol{\varepsilon}_E^*$ is the unique solution of the above modified Lippmann–Schwinger equation which is in $\boldsymbol{L}^2_{\text{ext}}(\Omega)$ because it has been proved in Section 5.2 that $\boldsymbol{Z}(\boldsymbol{\varepsilon}^*) = 0$ with $\boldsymbol{\varepsilon}^* \in \boldsymbol{L}^2_{\text{ext}}(\Omega)$ if, and only if, $\boldsymbol{\varepsilon}^* = 0$.

We see that the pair $(\boldsymbol{\varepsilon}_E, \boldsymbol{\sigma}_E)$ defined by equations (82)-(83) is the unique solution of the homogenization problem (47) which is $\boldsymbol{C}_0$-extended. And the equations (82) and (84) can be seen as a suitable change of variables in the initial Lippmann–Schwinger equation leading to the use of the uniformly bounded tensor fields $\boldsymbol{\alpha}$, $\boldsymbol{C}^D$ and $\boldsymbol{C}^S$ in the modified Lippmann–Schwinger equation.

6.4. The AEM algorithm

Therefore, the AEM scheme can be reformulated to solve the modified Lippmann–Schwinger equation (89) instead of the initial one. It is initialized with $(\boldsymbol{\varepsilon}^*)^0 = 0$, $\boldsymbol{X}^0 = \boldsymbol{E}$ and the iteration for $n \geq 0$ is to compute $\boldsymbol{X}^{n+1}$ and $(\boldsymbol{\varepsilon}^*)^{n+1}$ as follows, until a stopping criterion is reached:

$$\boldsymbol{Z}^n = \boldsymbol{Z}(\boldsymbol{X}^n) \tag{91}$$

$$\lambda^n = \frac{\langle \boldsymbol{X}^n : \boldsymbol{C}_0 : \boldsymbol{Z}^n \rangle_\Omega}{\langle \boldsymbol{Z}^n : \boldsymbol{C}_0 : \boldsymbol{Z}^n \rangle_\Omega} \tag{92}$$

$$\boldsymbol{X}^{n+1} = \boldsymbol{X}^n - \lambda^n \boldsymbol{Z}^n, \tag{93}$$

$$(\boldsymbol{\varepsilon}^*)^{n+1} = (\boldsymbol{\varepsilon}^*)^n + \lambda^n \boldsymbol{X}^n \tag{94}$$

The main steps are summarized in Algorithm 1.

One can see that the AEM scheme necessitates the storage of one additional variable, namely the residual $\boldsymbol{X}$, when compared to the algorithm dedicated to the polarization scheme with damping parameter $\gamma \in [0, 1)$ described in [17], and actually two additional variables, namely $\boldsymbol{X}$ and $\boldsymbol{Z}$, in the special case $\gamma = 0$. Details concerning the choice of the reference and of the stopping criterion are discussed in Section 7.

Algorithm 1 The AEM algorithm

$\boldsymbol{\varepsilon} \leftarrow 0$
$\boldsymbol{X} \leftarrow \boldsymbol{E}$
repeat
  $\boldsymbol{Z} \leftarrow (\boldsymbol{C}^D - \boldsymbol{C}^S) : \boldsymbol{X}$
  $\boldsymbol{Z} \leftarrow \boldsymbol{\Gamma}^0 * \boldsymbol{Z}$ use standard FFT and the analytical expression of $\boldsymbol{\Gamma}^0$ in Fourier space.
  $\boldsymbol{Z} \leftarrow \boldsymbol{\alpha} : \boldsymbol{X} + \boldsymbol{Z}$
  $\lambda \leftarrow \langle \boldsymbol{X} : \boldsymbol{C}_0 : \boldsymbol{Z} \rangle_\Omega / \langle \boldsymbol{Z} : \boldsymbol{C}_0 : \boldsymbol{Z} \rangle_\Omega$
  $\boldsymbol{X} \leftarrow \boldsymbol{X} - \lambda \boldsymbol{Z}$
  $\boldsymbol{\varepsilon} \leftarrow \boldsymbol{\varepsilon} + \lambda \boldsymbol{X}$
until Convergence criterion met
$\boldsymbol{\varepsilon} \leftarrow \boldsymbol{\alpha} : \boldsymbol{\varepsilon}$
return $\boldsymbol{\varepsilon}$

6.5. Link with gradient-descent methods

It is important to emphasize that the $\boldsymbol{Z}$-operator is not symmetric and that its symmetric part can be identified with a positive definite quadratic form on $\boldsymbol{L}^2_{\text{ext}}(\Omega)$ as shown by the key equation (67). Let us define the potential J for any $\boldsymbol{\varepsilon}^*$ in $\boldsymbol{L}^2_{\text{sym}}(\Omega)$ by:

$$J(\boldsymbol{\varepsilon}^*) = \frac{1}{2} \langle \boldsymbol{X}(\boldsymbol{\varepsilon}^*) : \boldsymbol{C}_0 : \boldsymbol{X}(\boldsymbol{\varepsilon}^*) \rangle_\Omega \tag{95}$$

where $\boldsymbol{X}(\boldsymbol{\varepsilon}^*)$ is given by (90), (89) and (61). Then the AEM iteration writes: $(\boldsymbol{\varepsilon}^*)^{n+1} = (\boldsymbol{\varepsilon}^*)^n + \lambda^n \boldsymbol{X}((\boldsymbol{\varepsilon}^*)^n)$ where λ^n minimizes $J((\boldsymbol{\varepsilon}^*)^{n+1})$.

Hence, the proposed AEM-scheme is *not* a gradient-descent method. For $n \geq 0$, $(\boldsymbol{\varepsilon}^*)^{n+1}$ is actually a linear combination of the fields $\boldsymbol{K}^0, \boldsymbol{K}^1, ..., \boldsymbol{K}^n$ where $\boldsymbol{K}^0 = \boldsymbol{E}$ and $\boldsymbol{K}^{i+1} = \boldsymbol{Z}(\boldsymbol{K}^i)$ for $i \geq 0$. So, it is a kind of Generalized Minimal RESsidual method (GMRES), but without any orthogonalization of the Krylov subspace generated by $\boldsymbol{K}^0, \boldsymbol{K}^1, ..., \boldsymbol{K}^n$.

In the spirit of [21], the solution of (89) could be found by minimizing J using some gradient method. Indeed, the minimizers of J, which are not necessarily in $\boldsymbol{L}^2_{\text{ext}}(\Omega)$, are such that $\boldsymbol{X}(\boldsymbol{\varepsilon}^*) = 0$ and $\nabla J(\boldsymbol{\varepsilon}^*) = 0$, where ∇J denotes the gradient of J. So, we have used a conjugate gradient method with zero initialization to solve $\nabla J(\boldsymbol{\varepsilon}^*) = 0$. The reader can find the expression of ∇J in Appendix E. The numerical simulations with this scheme were disappointing compared with those conducted with the AEM scheme. Indeed, unlike AEM, for some choices of reference material this scheme fails to converge, probably because the solution is not unique in the pores nor in the rigid inclusions (one of the main features of AEM is to select the unique solution in $\boldsymbol{L}^2_{\text{ext}}(\Omega)$) . In addition, two convolutions are required for each iteration instead of one for the AEM scheme. In conclusion, there is no advantage in using this scheme instead of AEM.

6.6. Useful expressions of $\boldsymbol{C}_{\text{hom}}$

It is also convenient to introduce the modified fourth-order strain-localization tensor field $\boldsymbol{A}^*(\boldsymbol{y}) = (A^*_{ijkl}(\boldsymbol{y}))$ that maps $\boldsymbol{E}$ onto $\boldsymbol{\varepsilon}^*_E(\boldsymbol{y})$:

$$\boldsymbol{\varepsilon}^*_E(\boldsymbol{y}) = \boldsymbol{A}^*(\boldsymbol{y}) : \boldsymbol{E}. \tag{96}$$

Recall that the localization tensor $\boldsymbol{A}$ of the initial homogenization problem is defined only in the matrix. Then, one can write $\boldsymbol{A} = \boldsymbol{\alpha} : \boldsymbol{A}^*$ in the matrix, and using this equation one can extend $\boldsymbol{A}$ to the whole unit cell. Moreover, inserting (82) into equation $\langle \boldsymbol{\sigma}_E : \boldsymbol{\varepsilon}_E \rangle_\Omega = \langle \boldsymbol{\sigma}_E \rangle_\Omega : \langle \boldsymbol{\varepsilon}_E \rangle_\Omega = \langle \boldsymbol{\sigma}_E \rangle_\Omega : \boldsymbol{E}$ which is true for any $\boldsymbol{E}$, one obtains the following expressions of $\boldsymbol{C}_{\text{hom}}$:

$$\boldsymbol{C}_{\text{hom}} = \langle \boldsymbol{C}^D : \boldsymbol{A}^* \rangle_\Omega = \langle (\boldsymbol{A}^*)^t : \boldsymbol{C}^* : \boldsymbol{A}^* \rangle_\Omega \tag{97}$$

where $\boldsymbol{C}^* = 0$ in the pores and in the rigid inclusions and

$$\boldsymbol{C}^* = \boldsymbol{\alpha}^t : \boldsymbol{C} : \boldsymbol{\alpha} = 4\boldsymbol{C}_0 : (\boldsymbol{C} + \boldsymbol{C}_0)^{-1} : \boldsymbol{C} : (\boldsymbol{C} + \boldsymbol{C}_0)^{-1} : \boldsymbol{C}_0 \tag{98}$$

in the matrix.

Now, taking the average of $\boldsymbol{\varepsilon}_E^*$ and using (84), we have:

$$\langle \boldsymbol{\varepsilon}_E^* \rangle_\Omega = \langle \boldsymbol{A}^* \rangle_\Omega : \boldsymbol{E} = \frac{1}{2}\left((\boldsymbol{C}_0)^{-1} : \boldsymbol{C}_{\text{hom}} + \boldsymbol{I} \right) : \boldsymbol{E}. \tag{99}$$

Remarkably, if the reference medium, $\boldsymbol{C}_0$, coincides with the homogenized one, $\boldsymbol{C}_{\text{hom}}$, then we will have $\langle \boldsymbol{A}^* \rangle_\Omega = \boldsymbol{I}$, which means that the average of $\boldsymbol{\varepsilon}_E^*$ is equal to $\boldsymbol{E}$ for any $\boldsymbol{E}$.

It is also interesting to compute the average of $\boldsymbol{\varepsilon}_E^*$ over the pores, $\langle \boldsymbol{\varepsilon}_E^* \rangle_{\Omega^p}$, and its average over the rigid inclusions, $\langle \boldsymbol{\varepsilon}_E^* \rangle_{\Omega^r}$. Using equations (82) and (84), we have:

$$\langle \boldsymbol{\varepsilon}_E \rangle_{\Omega^p} = \langle \boldsymbol{\alpha} : \boldsymbol{\varepsilon}_E^* \rangle_{\Omega^p} = 2\langle \boldsymbol{\varepsilon}_E^* \rangle_{\Omega^p}, \quad \langle \boldsymbol{\sigma}_E \rangle_{\Omega^r} = 2\boldsymbol{C}_0 : \langle \boldsymbol{\varepsilon}_E^* \rangle_{\Omega^r}. \tag{100}$$

Since $\langle \boldsymbol{\varepsilon}_E \rangle_{\Omega^p}$ and $\langle \boldsymbol{\sigma}_E \rangle_{\Omega^r}$ are independent of the choice of the reference medium, $\boldsymbol{C}_0$, it is found that $\langle \boldsymbol{\varepsilon}_E^* \rangle_{\Omega^p}$ is independent of $\boldsymbol{C}_0$ and $\langle \boldsymbol{\varepsilon}_E^* \rangle_{\Omega^r}$ behaves like the inverse of $\boldsymbol{C}_0$.

7. Implementation of the AEM iterations

We have shown that the zero-initialization proposed above leads to the selection of a solution with a certain regularity. In our implementation of the method, we have systematically used this initialization, which allows some optimizations, discussed in this paragraph.

7.1. Choosing the reference medium

We have already proved that the AEM scheme is unconditionally linearly convergent for any choice of the reference medium and we have interpreted this algorithm as a variable change which allows to use uniformly bounded tensors in the modified Lippmann–Schwinger equation.

Moreover, the previous analysis shows that if one wants to minimize auxiliary strain variations on the unit cell, then the reference medium should be of the same order as the unknown homogenized medium. That is why it is reasonable to choose a reference medium of the same order of the expected homogenized medium.

Another way of dealing with the issue is to remember that the rate of convergence of the AEM scheme is governed by the $\boldsymbol{C}_0$-dependent value of a_0^- introduced by equation (75). An alternative idea is therefore to choose $\boldsymbol{C}_0$ in such a way as to minimize a_0^-. However, a_0^- is not explicitly known. We have only the upper bound in (80) involving the constants c and d, and we are reduced to optimizing this bound. Therefore, we should keep in mind that this optimization will only give an indication of the rate of convergence.

We consider $\boldsymbol{C}_0$ of the form $\boldsymbol{C}_0 = k_0 \boldsymbol{C}_*$ where $\boldsymbol{C}_*$ is a fixed given stiffness tensor and k_0 is a positive multiplying constant which must be optimized. It can be seen that the constant c which appears in (51) and (80) is not k_0-dependent. On the other hand, assume that the uniform coercivity condition holds true for $\boldsymbol{C}_*$, μ_*^- and μ_*^+ in (9) instead of $\boldsymbol{C}_0$, μ^- and μ^+, respectively. Then, the constant d in (78) and (80) has the following form for $\boldsymbol{C}_0 = k_0 \boldsymbol{C}_*$:

$$d = \min\left\{ \frac{2}{1 + \frac{\mu_*^+}{k_0}}, \frac{2\frac{\mu_*^-}{k_0}}{1 + \frac{\mu_*^-}{k_0}} \right\}. \tag{101}$$

Its maximum value

$$d^+ = \frac{2\sqrt{\mu_*^-}}{\sqrt{\mu_*^+} + \sqrt{\mu_*^-}} \tag{102}$$

is reached for the optimum value of k_0, k_0^{opt}, given by:

$$k_0^{\text{opt}} = \sqrt{\mu_*^+ \mu_*^-}. \tag{103}$$

In the case of a homogeneous matrix, $\boldsymbol{C}(\boldsymbol{y}) = \boldsymbol{C}_*$ for all $\boldsymbol{y}$ in Ω^{m}, then $k_0^{\text{opt}} = 1$, which means that the optimum reference medium is the matrix itself. Moreover, if $k_0/k_0^{\text{opt}} \ll 1$ or $k_0/k_0^{\text{opt}} \gg 1$, then $d \ll 1$ which indicates that the convergence rate could deteriorate a lot in these cases.

To better characterize these limit cases, consider $\boldsymbol{C}_0$ of the form $\boldsymbol{C}_0 = k_0\boldsymbol{C}_*$ and a pair of strain-stress fields, $(\boldsymbol{\varepsilon}, \boldsymbol{\sigma}) \in \boldsymbol{L}^2_{\text{sym}}(\Omega) \times \boldsymbol{L}^2_{\text{sym}}(\Omega)$, complying to the constitutive equations (46). Let λ be the corresponding relaxation parameter according to the AEM scheme (62), where the residual, $\boldsymbol{X}$, and the direction, $\boldsymbol{Z}$, are respectively given by (49) and (61) where we assume that $\boldsymbol{Z} \neq 0$. For $k_0 \to +\infty$ or $k_0 \to 0$ and $(\boldsymbol{\varepsilon}, \boldsymbol{\sigma})$ being fixed, we find that λ goes to the same limit:

$$\lambda \to \frac{1}{2}, \tag{104}$$

from which we see that λ staying close to $\frac{1}{2}$ for many successive iterations is an indication that the reference medium is too soft or too stiff.

7.2. Stopping criteria

Let $(\boldsymbol{\varepsilon}, \boldsymbol{\sigma}) \in \boldsymbol{L}^2_{\text{sym}}(\Omega) \times \boldsymbol{L}^2_{\text{sym}}(\Omega)$ be a pair of strain-stress fields which complies with the constitutive equations (46). It can be considered as a good approximation of the solution to the homogenization problem if its residual (49) is small enough. Thanks to the orthogonal decomposition of this residual (50), one can write:

$$\|\boldsymbol{X}\|^2_{\boldsymbol{C}_0} = \| (\boldsymbol{E} - \boldsymbol{\varepsilon})^S \|^2_{\boldsymbol{C}_0} + \| \left(\boldsymbol{C}_0^{-1} : \boldsymbol{\sigma}\right)^D \|^2_{\boldsymbol{C}_0}. \tag{105}$$

There are two contributions to the residual: the error in compatibility, $\| (\boldsymbol{E} - \boldsymbol{\varepsilon})^S \|_{\boldsymbol{C}_0}$, and the error in equilibrium, $\| \left(\boldsymbol{C}_0^{-1} : \boldsymbol{\sigma}\right)^D \|_{\boldsymbol{C}_0}$. When these errors are not zero, their relative importance depends on the choice of the reference medium $\boldsymbol{C}_0$: as $\boldsymbol{C}_0$ increases, the relative contribution of the error in equilibrium to the residual decreases, and as $\boldsymbol{C}_0$ decreases, the relative contribution of the error in equilibrium to the residual increases. Since in the AEM scheme the strain is not compatible, nor the stress is in equilibrium, one has to ensure that both the projection of $\boldsymbol{E} - \boldsymbol{\varepsilon} \neq 0$ on S and the projection of $\boldsymbol{C}_0^{-1} : \boldsymbol{\sigma} \neq 0$ on D are small enough. We therefore introduce:

$$\Delta^S = \frac{\| (\boldsymbol{E} - \boldsymbol{\varepsilon})^S \|_{\boldsymbol{C}_0}}{\|\boldsymbol{E} - \boldsymbol{\varepsilon}\|_{\boldsymbol{C}_0}} \tag{106}$$

$$\Delta^D = \frac{\| \left(\boldsymbol{C}_0^{-1} : \boldsymbol{\sigma}\right)^D \|_{\boldsymbol{C}_0}}{\|\boldsymbol{C}_0^{-1} : \boldsymbol{\sigma}\|_{\boldsymbol{C}_0}} \tag{107}$$

as the normalized compatibility and equilibrium errors, respectively. Clearly, if $\boldsymbol{C}_0$ is of the form $\boldsymbol{C}_0 = k_0\boldsymbol{C}_*$, then $0 \leq \Delta^S \leq 1$ and $0 \leq \Delta^D \leq 1$ are not k_0-dependent. Concerning the equilibrium error, we avoid using the L^2-norm of the divergence of $\boldsymbol{\sigma}$ because, in the general case, there is no guarantee that this divergence is in L^2.

A possible stopping criterion of the AEM scheme can therefore be $\Delta = \max\{\Delta^S, \Delta^D\} \leq \texttt{tol}$ where `tol` is a user-prescribed relative tolerance.

At first sight, the computation of Δ^S, Δ^D should require the use of additional convolutions at each iteration. In reality, this is not the case if we organize the algorithm as described in Appendix F. In this alternative version of the algorithm, Δ^S, Δ^D can be computed from the intermediate results of the algorithm steps. The AEM algorithm, including the compatibility/equilibrium errors computation, still requires one single convolution per iteration.

It should be mentioned that the discretization of the Green operator has a huge influence on whether a particular solution scheme converges or not in case of infinite contrast. Actually, there are discretizations which do not inherit the salient properties of the continuous case. In the next section, we are also going to numerically test the robustness of our scheme in relation to the discretization.

8. Illustrative applications

The AEM scheme has been implemented in the Janus Python library[2]. For the Green operator discretization scheme, unless stated otherwise, we use the finite differences scheme proposed in [25] which results in improved accuracy of the local fields over more classical discretization strategies.

[2] Available at https://github.com/sbrisard/janus

8.1. 2D matrix-inclusion microstructure

In this section, we consider a 2D microstructure consisting of a stiff circular inclusion of radius 0.25 (phase 2) embedded in a matrix (phase 1). Both media have zero Poisson ratio $\nu_1 = \nu_2 = 0$ and the matrix has a shear modulus $G_1 = 1$. The RVE is discretized with a $N \times N$ grid with $N = 128$ unless stated otherwise and the loading consists of a uniaxial unit strain $\boldsymbol{E} = \boldsymbol{e}_x \otimes \boldsymbol{e}_x$. Finally, we choose $G_0 = G_1$ and $\nu_0 = 0$ for the reference medium.

We first investigate the performance of the AEM algorithm when varying the inclusion stiffness G_2. We test in particular the perfectly rigid case where $G_2 = \infty$ since AEM is perfectly able to handle such a limit case. Convergence results are reported in Figure 1 in terms of the average energy $\langle \boldsymbol{\sigma} : \boldsymbol{\varepsilon} \rangle_\Omega$, the total residual:

$$\texttt{residual} = \frac{\|\boldsymbol{X}\|_{\mathbb{C}_0}}{\|\boldsymbol{E}\|_{\mathbb{C}_0}} \tag{108}$$

and the normalized compatibility and equilibrium residuals Δ^S, Δ^D (106)-(107).

Results first indicate that AEM succeeds in converging in all cases. In particular, the convergence of the energy is extremely fast since a stabilized value is reached in roughly 10 iterations, even in the challenging case of infinite contrast. When inspecting the various residual measures, we find that convergence is extremely fast for moderate values of the stiffness contrast where machine precision is reached within only a few tens of iterations. For larger stiffness contrasts, convergence to machine precision is reached for a few hundred of iterations. However, we must highlight that we still maintain a very good convergence rate even in the infinite case. Indeed, due to the specific scaling used in the AEM iterations, the algorithm behavior for a contrast between 100 and $+\infty$ is essentially the same.

To further assess the robustness of the AEM algorithm, we report in Figure 2 the evolution of the compatibility and equilibrium residuals for the two cases $G_2 = 2G_1$ and $G_2 = 1000G_1$ for varying grid sizes N. We can observe that both residuals decrease in a very similar manner irrespective of the chosen grid size, the convergence rate being essentially driven by the contrast ratio as discussed before.

8.2. 3-phase 2D medium with double contrast

In order to have a better understanding of the origin of the efficiency of the AEM algorithm, Figure 3 shows the evolution of the physical strain field $\boldsymbol{\varepsilon}$ and its auxiliary counterpart $\boldsymbol{\varepsilon}^*$ during the first iterations in the following double contrast case: a square microstructure consisting of a rigid circular inclusion of radius 0.25 (phase 2) located at the center of the domain and softer inclusions of radius 0.25 (phase 3) centered at the vertices of the square domain. The matrix (phase 1) has a Poisson ratio $\nu_1 = 0.3$ and a shear modulus $G_1 = 1$. The inclusions have the same Poisson ratio $\nu_1 = \nu_2 = \nu_3$ and different shear moduli G_2 and G_3. For simplicity, we take in the following $G_2 = \chi G_1$ and $G_3 = G_1/\chi$ where χ denotes the double contrast ratio between the stiff inclusions and the matrix and between the matrix and the soft inclusions. A 3D variant of this microstructure will be considered in the next section. The RVE is discretized with a 512×512 grid size, the loading consists of a uniaxial unit strain $\boldsymbol{E} = \boldsymbol{e}_x \otimes \boldsymbol{e}_x$, the contrast is infinite, $\chi = \infty$, and the reference material is the matrix.

First, we observe that $\boldsymbol{\varepsilon}^*$ exhibits a similar strain level in both the inclusion and the pore due to the re-scaling procedure. Indeed, we have chosen the reference material corresponding to the matrix properties. The latter are then relatively close to that of the homogenized medium, which implies that the average auxiliary strain in the pore and the rigid inclusions are of similar level as suggested by (100).

Second, we see that, after the very first iteration, the auxiliary strain is constant ($\boldsymbol{\varepsilon}^* = \lambda \boldsymbol{E}$) which corresponds to a physical strain being exactly zero in the rigid inclusion and being larger than the total average strain in the pore. This first step may be seen as a very efficient initialization procedure for the real physical strain. After the second iteration, intraphase heterogeneities are already well captured. The subsequent iterations then slightly update the strain field to satisfy both equilibrium and compatibility. After iteration 10, changes of the strain field become imperceptible to the naked eye.

8.3. 3-phase 3D medium with double contrast

In the following, we consider the 3D variant of the previous double inclusion setting with the same geometric and elastic parameters, see Figure 4. The RVE is discretized with a $32 \times 32 \times 32$ grid and the loading consists of a uniaxial

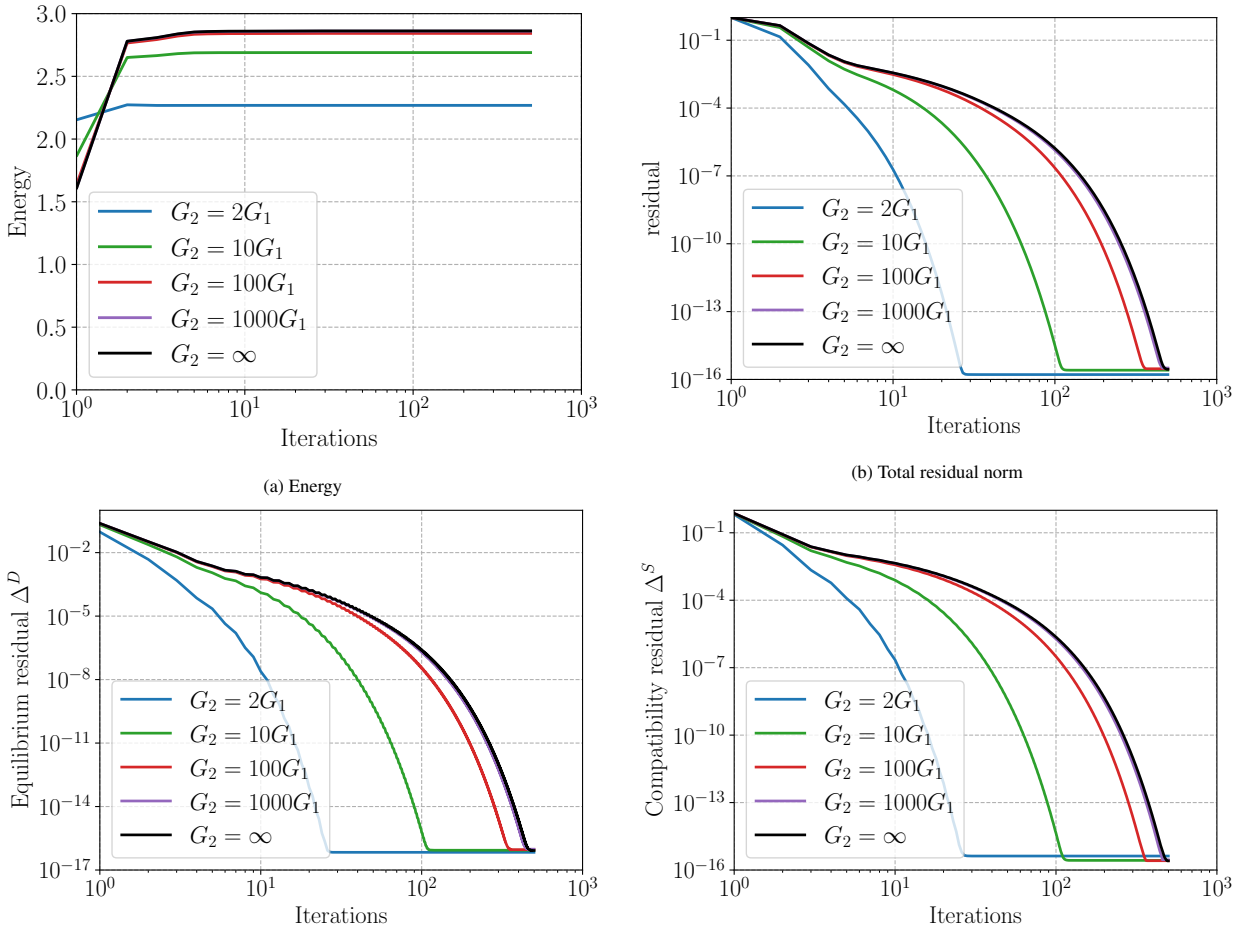

(a) Energy

(b) Total residual norm

(c) Equilibrium residual

(d) Compatibility residual

Figure 1: Convergence of AEM for various inclusion stiffness moduli in the 2D matrix-inclusion microstructure.

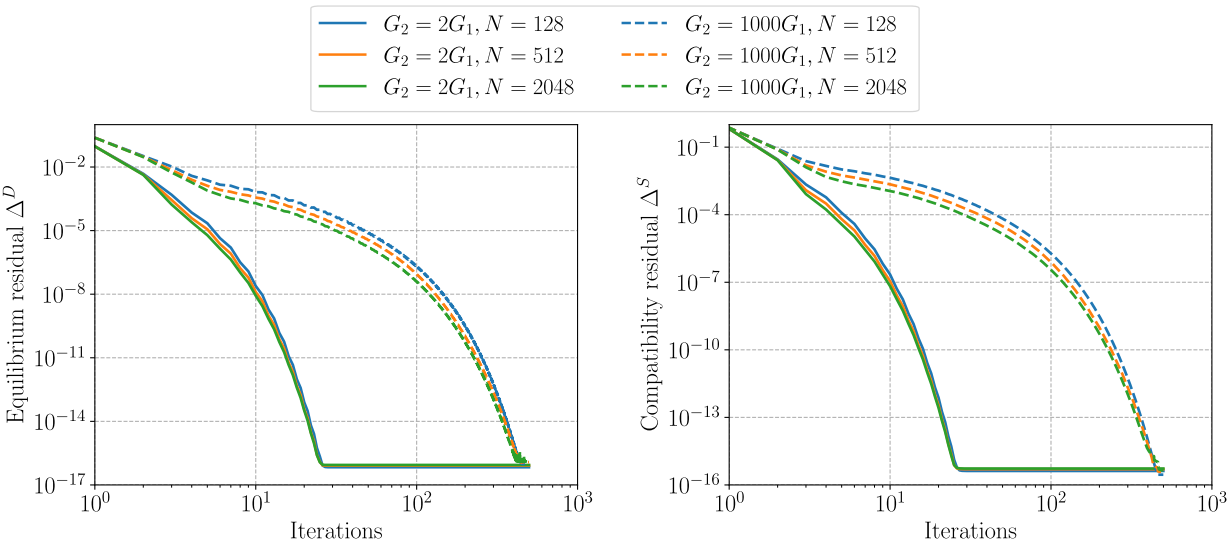

(a) Equilibrium residual

(b) Compatibility residual

Figure 2: Convergence of AEM for various grid size N in the 2D matrix-inclusion microstructure.

unit strain $\boldsymbol{E} = \boldsymbol{e}_x \otimes \boldsymbol{e}_x$.

In this section, we aim to assess the performance of the AEM algorithm compared to several classical schemes such as the basic Moulinec-Suquet (MS) scheme, the standard Eyre-Milton (EM) scheme and the Conjugate-Gradient (CG) scheme. For the CG scheme, we use the version introduced by Zeman et al. [9], that is independent of the choice of reference medium. In all above mentioned schemes, the strain field is initialized with $\boldsymbol{\varepsilon} = \boldsymbol{E}$. On the other hand, zero initialization of the strain field is adopted in the polarization schemes, parametrized with different values of $\gamma = 1 - \lambda$: $\gamma = 1/4$ (Monchiet-Bonnet), $\gamma = 1/2$ (augmented Lagrangian) and $\gamma = 0$ (Eyre-Milton with zero initialization). All schemes are implemented in the same framework as AEM using the Janus library. Finally, we adopt for the reference medium the following values which are usually suggested in the literature for the various schemes:

- the arithmetic average moduli (23) for MS
- the geometric average moduli (26) for EM and the polarization schemes. In this particular case of double inverse contrast, this amounts to choosing $G_0 = 1$ and $\nu_0 = 0.3$, that is the matrix elastic moduli.
- the matrix elastic moduli for CG and AEM.

In summary, the reference medium coincides with the matrix in all schemes, except MS. In each case, we compute the average energy and the following common normalized residual (even for MS):

$$\texttt{residual} = \frac{\sqrt{\| \left(\boldsymbol{E} - \boldsymbol{\varepsilon}\right)^S \|^2_{\boldsymbol{C}_m} + \| \left(\boldsymbol{C}_m^{-1} : \boldsymbol{\sigma}\right)^D \|^2_{\boldsymbol{C}_m}}}{\|\boldsymbol{E}\|_{\boldsymbol{C}_m}} \tag{109}$$

where $\boldsymbol{C}_m$ is the elasticity tensor of the matrix, and $\|.\|_{\boldsymbol{C}_m}$ its corresponding norm. In this way, we avoid introducing any bias in the evaluation of the convergence between schemes with different reference medium or different $\boldsymbol{E}$.

8.3.1. Comparison against classical schemes

For a moderate contrast $\chi = 10$, Figure 5 shows that all of the considered schemes converge quite rapidly to the solution with a relatively similar speed, except for the MS scheme which is slower than the other methods.

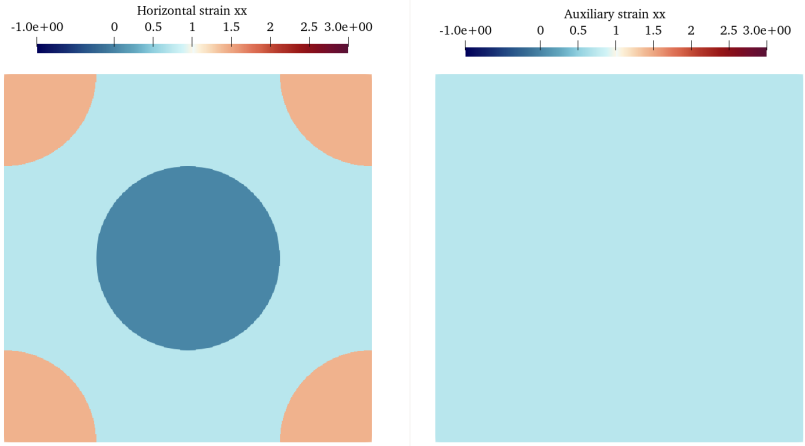

(a) Iteration 1

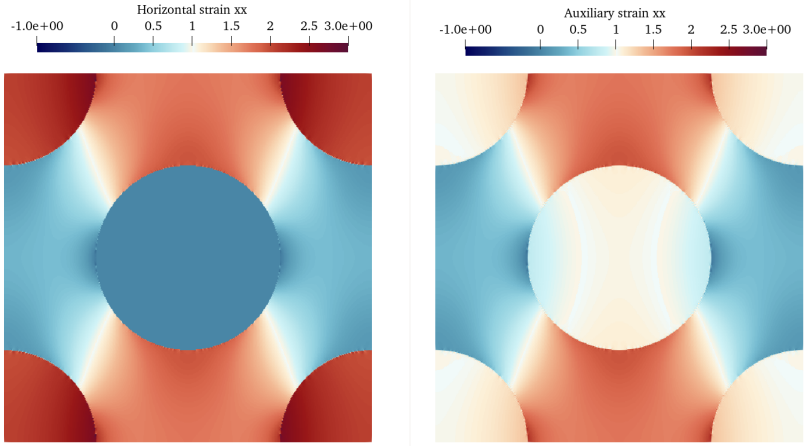

(b) Iteration 2

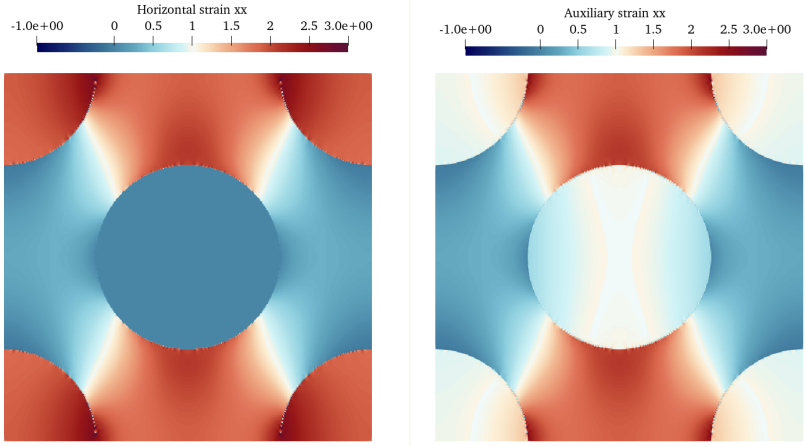

(c) Iteration 10 and beyond

Figure 3: Horizontal strain ε_{xx} (left) and auxiliary strain ε^*_{xx} (right) for the infinite contrast case in the 3-phase 2D microstructure with double contrast.

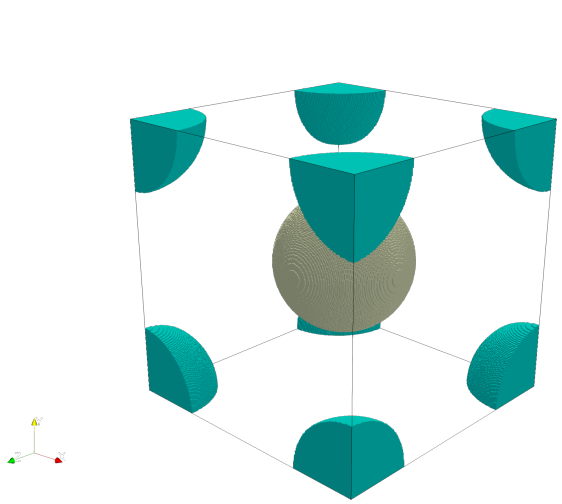

Figure 4: 3-phase 3D medium with double contrast. The pore is in light blue, the inclusion in grey and the matrix is hidden.

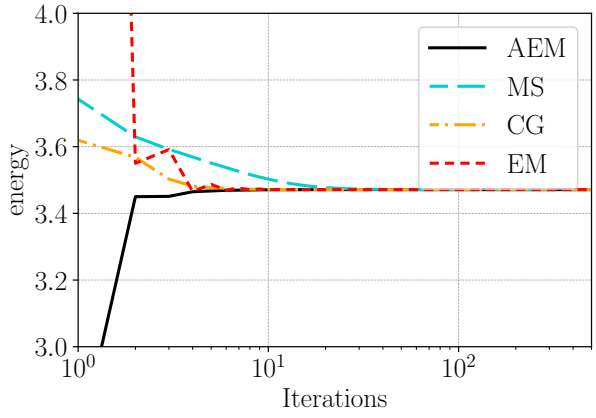

(a) Energy

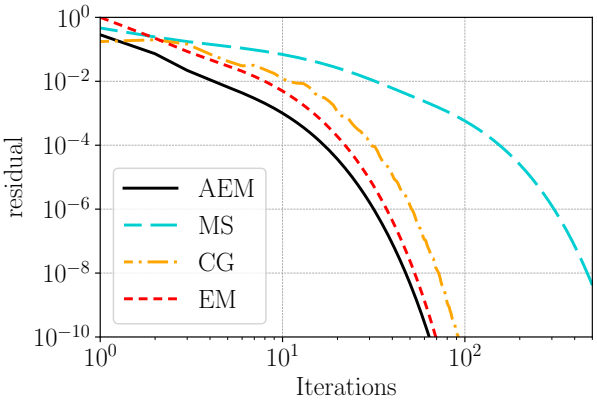

(b) Total residual

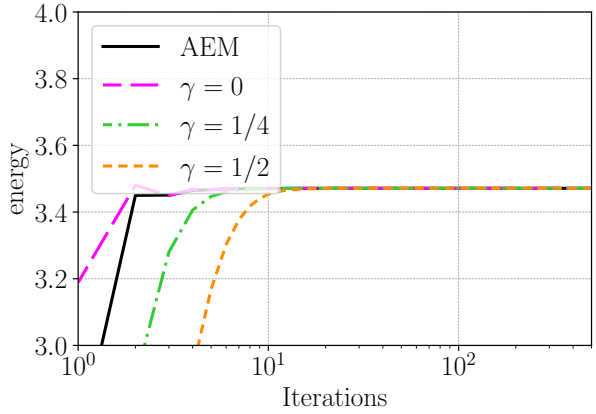

(c) Energy

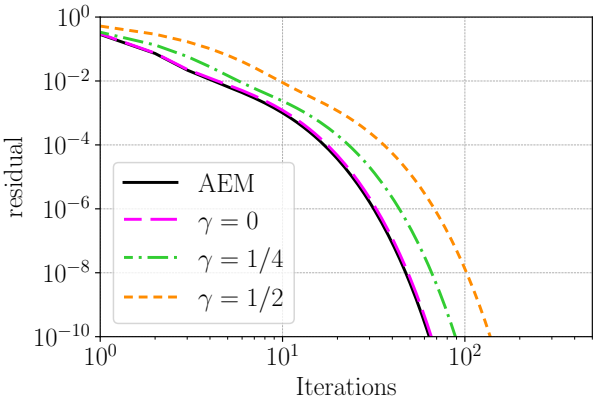

(d) Total residual

Figure 5: Convergence of MS, EM, CG, γ and AEM schemes in the double contrast 3D microstructure with $\chi = 10$

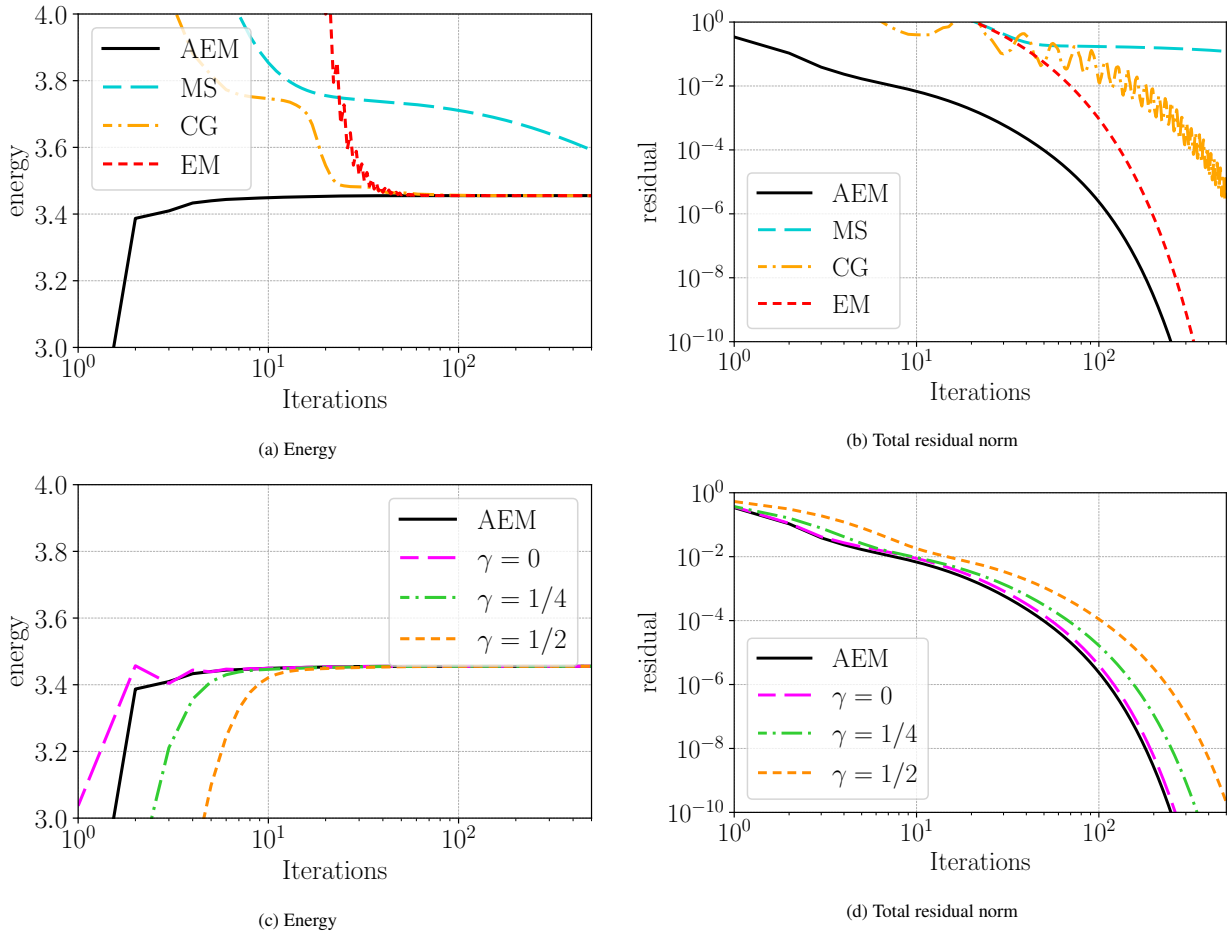

(a) Energy

(b) Total residual norm

(c) Energy

(d) Total residual norm

Figure 6: Convergence of MS, EM, CG , γ and AEM schemes in the double contrast 3D microstructure with $\chi = 1000$

The case of a stronger contrast $\chi = 1000$ is reported in Figure 6. In terms of energy, the convergence of AEM and $\gamma = 0$-scheme is faster than all of the other considered schemes, and also smoother than CG and EM for instance. When looking at the total residual, we can see that MS fails to substantially reduce the residual in this large contrast case. Moreover, AEM starts with a smaller value of the residual than EM due to a different choice for the initialization. Indeed, all the γ-schemes (for which the step-size is fixed) behave like AEM. As a result, the difference between EM and $\gamma = 0$-scheme is related to the initialization of the algorithm.

We now investigate the case of an infinite contrast $\chi = \infty$ with AEM and the polarization schemes since only these schemes are able to handle the exact infinite-contrast case as discussed in Section 4.1. Figure 7 shows that all these schemes converge. Clearly, the convergence of $\gamma = 0$ and AEM is very similar and it is a little better than the convergence of $\gamma = 1/4$ and $\gamma = 1/2$.

8.3.2. Influence of the discretization scheme

It is worth noting that the convergence behavior of the different schemes can also be strongly influenced by the choice made for discretizing the Green operator. For instance, Figure 8 shows the results for the double contrast with $\chi = 1000$ when using the original discretization introduced by Moulinec and Suquet [1, 2]. This so-called *truncated Green operator* is known to introduce parasitic oscillations around material interfaces. By comparison with Figure 6 obtained with the Willot discretization [25], the convergence worsens in all schemes when using instead the truncated Green operator. However, AEM and polarization schemes seem more robust than the other schemes.

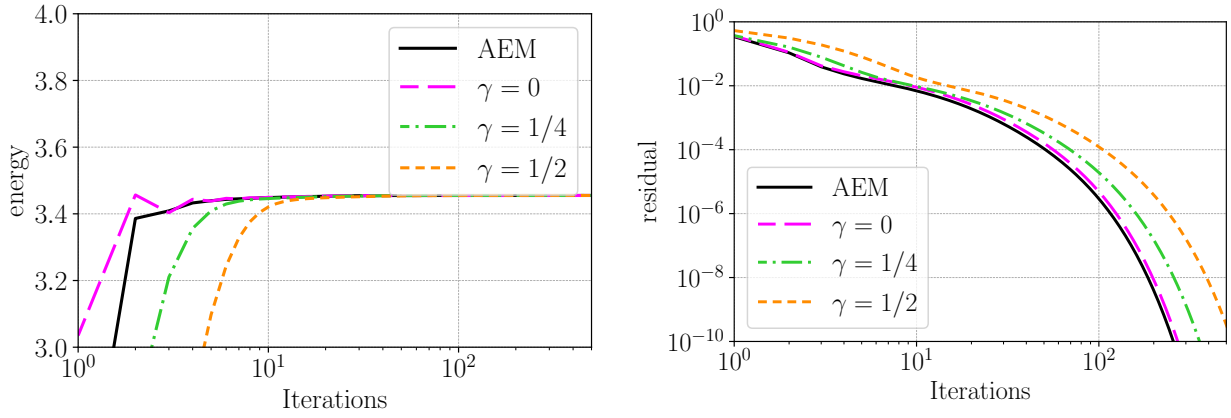

(a) Energy

(b) Total residual

Figure 7: Convergence of γ and AEM schemes in the double contrast 3D microstructure with $\chi = \infty$

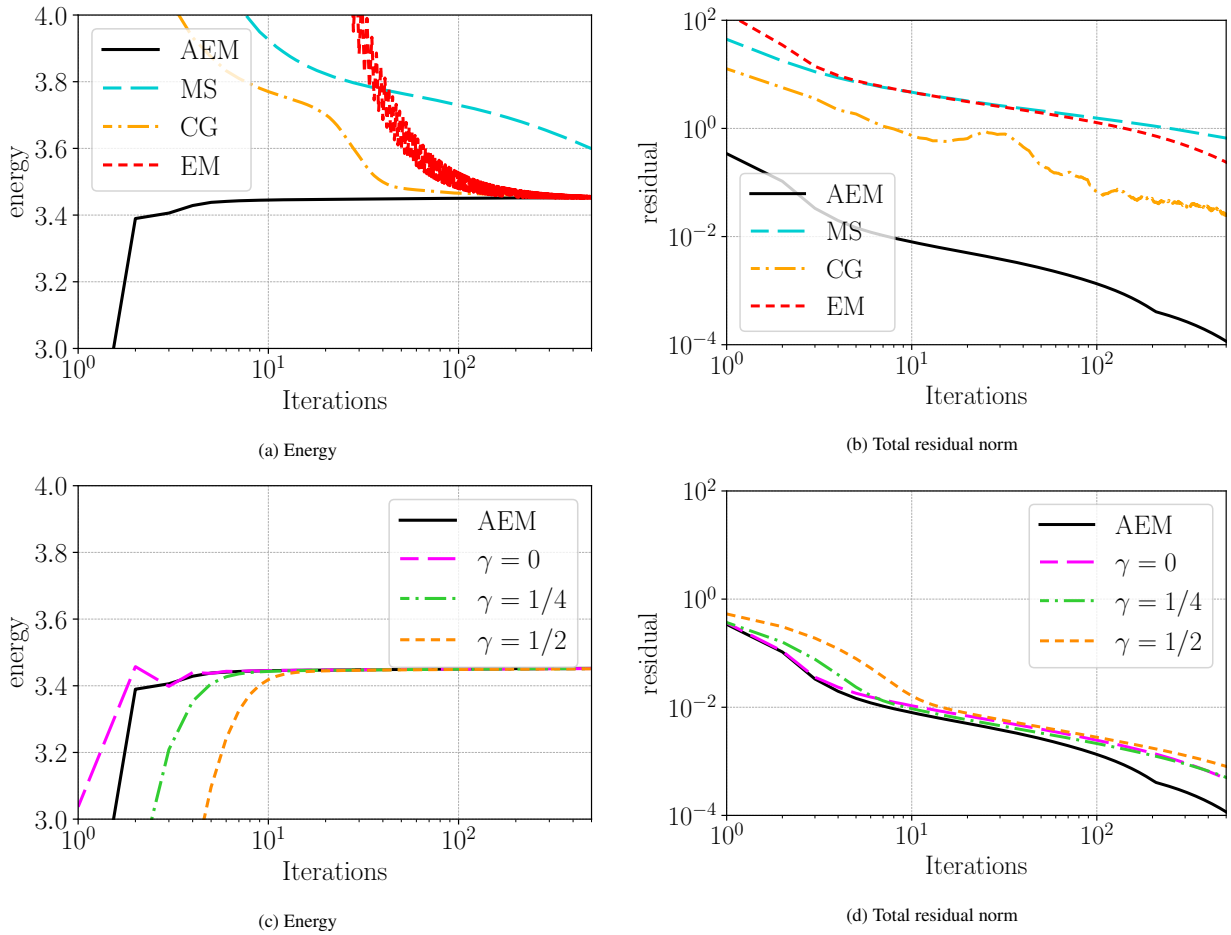

(a) Energy

(b) Total residual norm

(c) Energy

(d) Total residual norm

Figure 8: Convergence of MS, EM, CG , γ and AEM schemes in the double contrast 3D microstructure with $\chi = 1000$ using a truncated Green operator

8.3.3. Influence of the reference medium $\boldsymbol{C}_0$

Finally, we assess the influence of the choice of the reference medium $\boldsymbol{C}_0$ on the convergence behavior. For this purpose, we use the analysis and notations of Section 7.1. We consider $\boldsymbol{C}_0$ of the form $\boldsymbol{C}_0 = k_0\boldsymbol{C}_m$ where $\boldsymbol{C}_m$ is the stiffness of the matrix. We have already established that the optimal choice is $k_0^{\text{opt}} = 1$, i.e. to take the matrix as the reference medium. We want to assess the robustness of AEM and $\gamma = 0$ schemes as k_0 varies away from its optimal value for which both AEM and $\gamma = 0$ have similar convergence.

For this purpose, we consider first the double infinite contrast 3D case $\chi = \infty$ and vary k_0 for the AEM scheme. Figure 9 shows the convergence of AEM for $k_0 = 0.1$ and $k_0 = 10$. Here, the residual given by (109) is not k_0-dependent. It is observed that the convergence for $k_0 = 0.1$ and $k_0 = 10$ is slower than for the optimal choice $k_0 = k_0^{\text{opt}} = 1$ which further supports the theoretical convergence analysis of Section 5. Second, although the convergence for $k_0 = 0.1$ and $k_0 = 10$ are similar for the residuals, we observe that increasing k_0 worsens the convergence of the energy only slightly, whereas decreasing k_0 induce a larger deterioration of the convergence. We also observe that choosing a soft reference medium results in a slow evolution of the energy during the first iterations. Third, the evolution of the relaxation parameter λ is interesting. We observe oscillations of the relaxation parameter λ around 1 for $k_0 = k_0^{\text{opt}}$. We attribute this behavior to the fact that the convergence is reached very quickly and that the exact value of λ becomes meaningless. Remarkably, for $k_0 = 10k_0^{\text{opt}}$, λ is close to $1/2$ for the first iterations before reaching a value close to 1. Finally, for $k_0 = 0.1k_0^{\text{opt}}$, λ is close to 1.

In Figure 10 we compare the convergence of the AEM and $\gamma = 0$ schemes for a reference medium softer than the optimum one. We take $k_0 = 0.1k_0^{\text{opt}}$ and $k_0 = 0.01k_0^{\text{opt}}$. It is observed that both AEM and $\gamma = 0$ schemes predict the same energy. As for the corresponding normalized error Δ defined in Section 7.2, both schemes converge with a slightly better convergence for AEM scheme in the case $k_0 = 0.01k_0^{\text{opt}}$.

In Figure 11 we compare the convergence of the AEM and $\gamma = 0$ schemes for a reference medium stiffer than the optimum one. We take $k_0 = 10k_0^{\text{opt}}$ and $k_0 = 100k_0^{\text{opt}}$. It is observed that the energy predicted by the $\gamma = 0$ scheme strongly oscillates for the first iterations, and that these oscillations are amplified as k_0 increases. Moreover, the corresponding normalized error Δ defined in Section 7.2 seems constant (over the first 500 iterations) for $k_0 = 100k_0^{\text{opt}}$, which indicates that the convergence of the $\gamma = 0$ scheme is lost in this case. On the other hand AEM is still convergent and regular, even for such extreme choice of the reference medium.

Finally, we report in Figure 12 the evolution of the relaxation parameter λ for $k_0 = 0.001k_0^{\text{opt}}, 0.01k_0^{\text{opt}}, 100k_0^{\text{opt}}, 1000k_0^{\text{opt}}$. It is observed that, as predicted by the theoretical analysis, λ is close to $1/2$ for the first iterations, then it increases and stabilizes close to 1.

Let's summarize the findings of our numerical study in a few words. Polarization-based schemes are more suitable for highly contrasted microstrucures than MS, CG and EM schemes if the reference medium is correctly chosen. Among them, $\gamma = 0$ and AEM schemes are very comparable and they are the 'best'. However, the $\gamma = 0$ scheme loses convergence if the reference medium is chosen incorrectly, whereas AEM scheme linearly converges unconditionally for any choice of reference medium.

9. Conclusions

We proposed the so-called *Adaptive Eyre–Milton scheme (AEM)*, a novel iterative method for the numerical solution of the Lippmann–Schwinger equation with periodic boundary conditions for the case of linear constitutive equations. This scheme is derived from the classical Eyre–Milton scheme [6] and the polarization-based schemes [8], where at each iteration, the *direction* of the increment is preserved, while its *amplitude* is optimized. The main contributions of the present paper are summarized below.

1. The AEM, as well as the classical Eyre-Milton and the polarization-based schemes, have all been formulated in terms of the residual $\boldsymbol{X}$ rather than the strain field or the polarization.
2. This reformulation relies on rescaled auxiliary quantities which remain well-defined in the limit case of infinitely soft and infinitely stiff materials.
3. This translates numerically to exceptional robustness to large contrast of material properties with the ability to handle *exactly* zero (pores) and infinite (rigid inclusions) elastic moduli. This is the case for both the AEM and the polarization, thus including in particular the EM scheme ($\gamma = 0$) with a zero initialization.

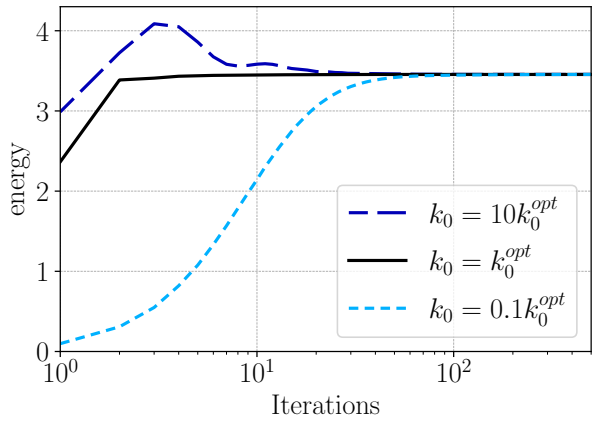

(a) Energy

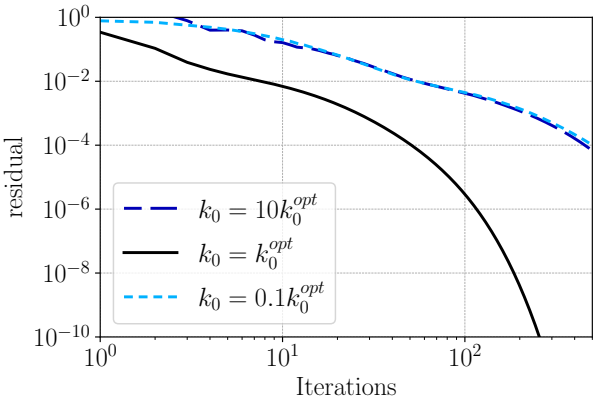

(b) Total residual norm

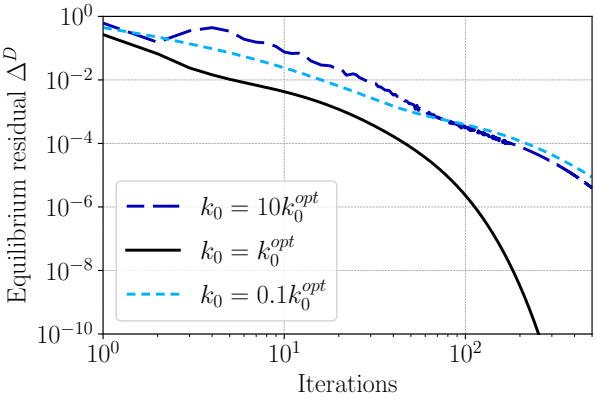

(c) Equilibrium residual

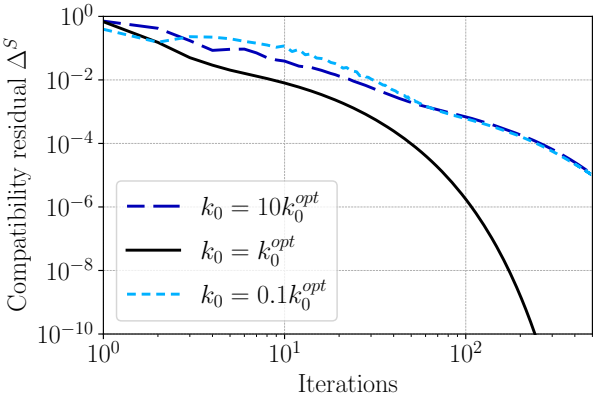

(d) Compatibility residual

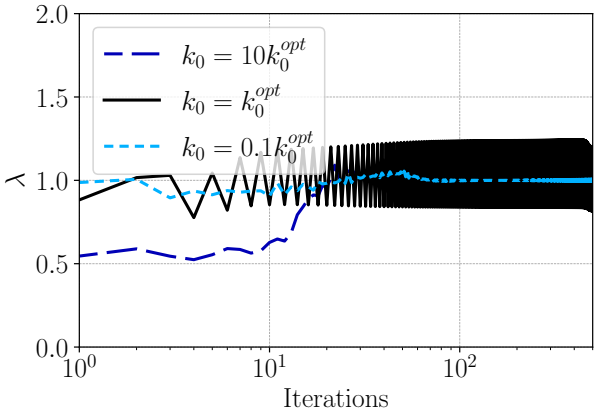

(e) Relaxation parameter λ

Figure 9: Influence of the choice of the reference medium on the convergence of AEM scheme for the 3D double-contrast microstructure with $\chi = \infty$.

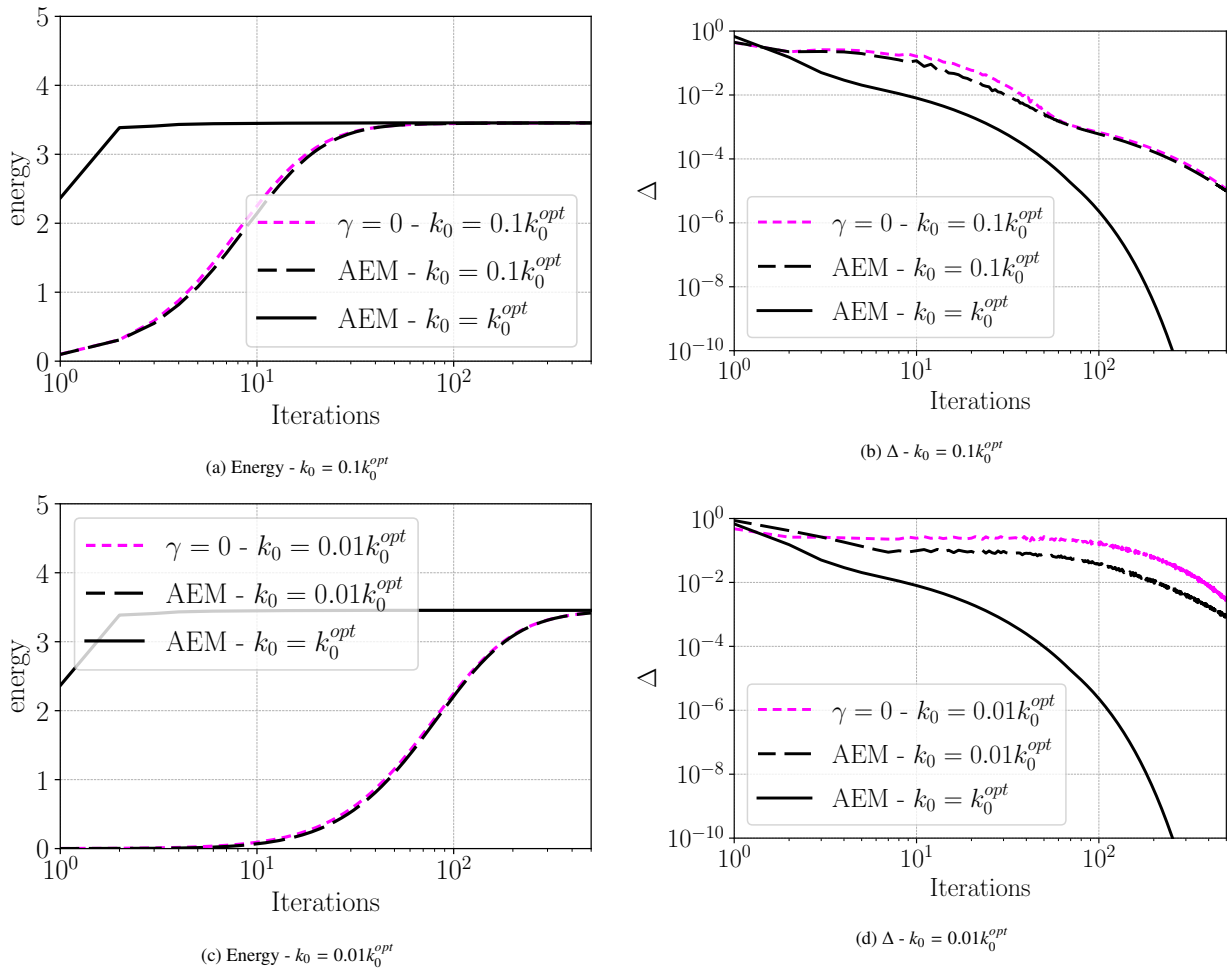

(a) Energy - $k_0 = 0.1k_0^{opt}$

(b) Δ - $k_0 = 0.1k_0^{opt}$

(c) Energy - $k_0 = 0.01k_0^{opt}$

(d) Δ - $k_0 = 0.01k_0^{opt}$

Figure 10: Comparison of the convergence of AEM and $\gamma = 0$ schemes for very soft reference media in the 3D double-contrast microstructure with $\chi = \infty$.

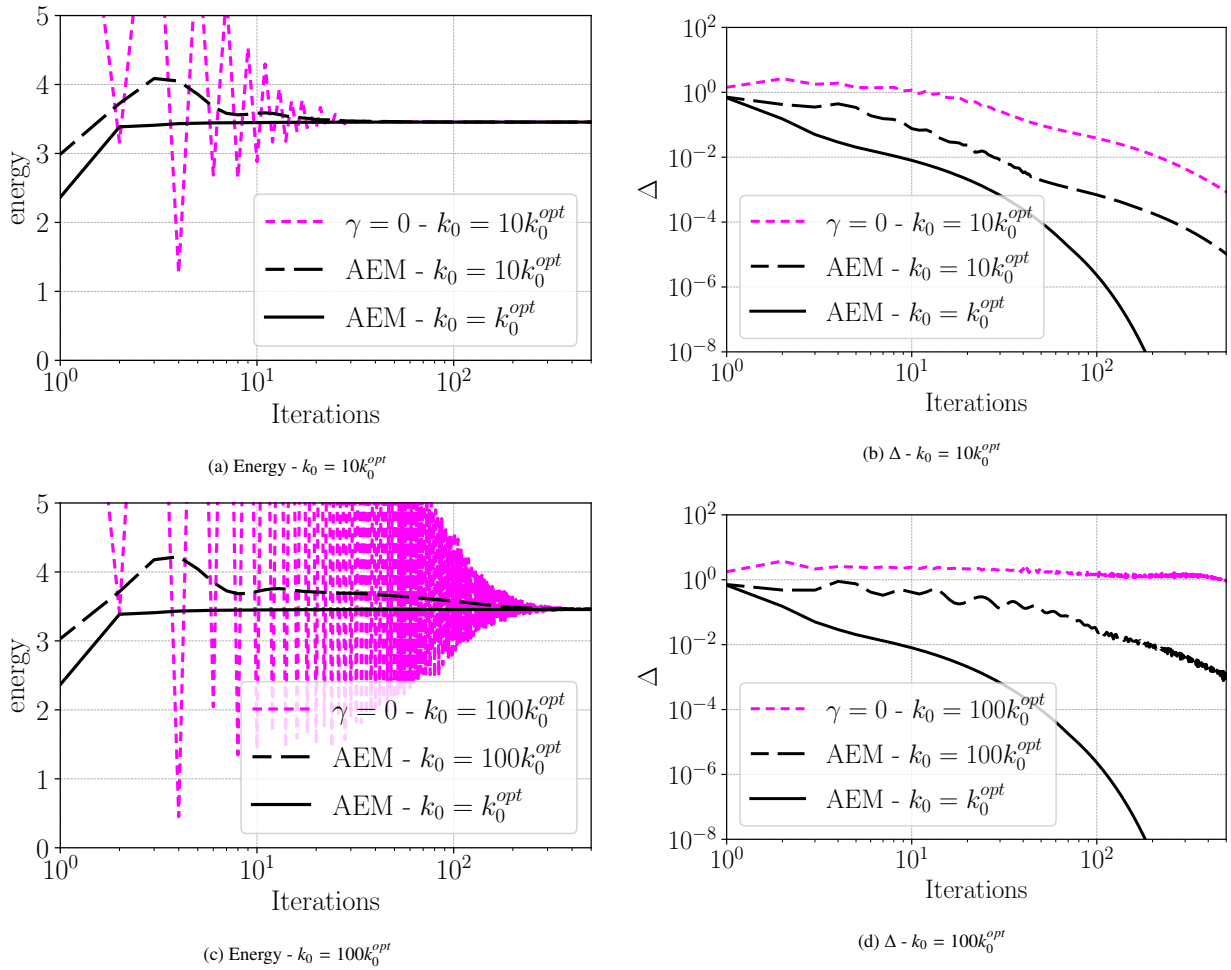

(a) Energy - $k_0 = 10k_0^{opt}$

(b) Δ - $k_0 = 10k_0^{opt}$

(c) Energy - $k_0 = 100k_0^{opt}$

(d) Δ - $k_0 = 100k_0^{opt}$

Figure 11: Comparison of the convergence of AEM and $\gamma = 0$ schemes for very stiff reference media in the 3D double-contrast microstructure with $\chi = \infty$.

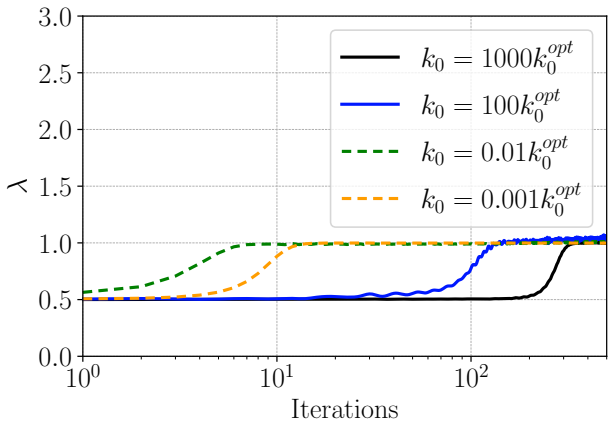

Figure 12: Evolution of the relaxation parameter λ in the AEM scheme for very stiff or very soft reference medium in the 3D double-contrast microstructure with $\chi = \infty$.

Focusing more particularly on the properties of the proposed AEM scheme, our main findings are as follows:

1. Intermediate steps of the algorithm provide, at no additional time cost, equilibrium and compatibility residual which can be used to check convergence.
2. Our simulations have shown weaker sensitivity of the AEM scheme's convergence to the spatial discretization (discrete Green operator) than other methods and almost insensitivity to the grid size.
3. Linear convergence is guaranteed for *any* value of the reference medium.
4. Optimal convergence rates seem to be associated with reference properties close to that of the connected phase or to that of the homogenized medium.
5. Initialization can be arbitrary. The proposed zero-initialization is both simple and allows to handle all the limit cases of porous and/or infinitely stiff materials.

This work opens a number of perspectives: we identified in particular two possible extensions. First, the AEM will be applied to nonlinear materials, where its robustness with respect to the material contrast will be particularly helpful. Second, we will work on an automatic or adaptive selection of the reference medium in the future. The preliminary observations stated in the present paper indeed point at optimal values that differ from that of the traditional MS and EM schemes.

CRediT authorship contribution statement

Karam Sab: Conceptualization, Formal analysis, Investigation, Methodology, Writing **Jérémy Bleyer**: Data curation, Software, Validation, Visualization, Writing **Sébastien Brisard**: Software, Writing - Review & Editing **Martin Dolbeau**: Data curation, Software, Validation, Visualization

Data availability

The scripts used to produce the results presented in the paper can be found at https://doi.org/10.5281/zenodo.10566496 [26].

References

[1] H. Moulinec, P. Suquet, A fast numerical method for computing the linear and nonlinear mechanical properties of composites, Comptes rendus de l'Académie des sciences. Série II, Mécanique, physique, chimie, astronomie 318 (11) (1994) 1417–1423.

[2] H. Moulinec, P. Suquet, A numerical method for computing the overall response of nonlinear composites with complex microstructure, Computer Methods in Applied Mechanics and Engineering 157 (1–2) (1998) 69–94. doi:10.1016/S0045-7825(97)00218-1.

[3] J. Korringa, Theory of elastic constants of heterogeneous media, Journal of Mathematical Physics 14 (4) (1973) 509–513. doi:doi:10.1063/1.1666346.

[4] R. Zeller, P. H. Dederichs, Elastic Constants of Polycrystals, Physica Status Solidi (B) 55 (2) (1973) 831–842. doi:10.1002/pssb.2220550241.

[5] E. Kröner, On the Physics and Mathematics of Self-Stresses, in: J. L. Zeman, F. Ziegler (Eds.), Topics in Applied Continuum Mechanics, Springer Verlag Wien, Vienna, 1974, pp. 22–38.

[6] D. J. Eyre, G. W. Milton, A fast numerical scheme for computing the response of composites using grid refinement, The European Physical Journal - Applied Physics 6 (01) (1999) 41–47. doi:10.1051/epjap:1999150.

[7] J. C. Michel, H. Moulinec, P. Suquet, A computational scheme for linear and non-linear composites with arbitrary phase contrast, International Journal for Numerical Methods in Engineering 52 (1-2) (2001) 139–160. doi:10.1002/nme.275.

[8] V. Monchiet, G. Bonnet, A polarization-based FFT iterative scheme for computing the effective properties of elastic composites with arbitrary contrast, International Journal for Numerical Methods in Engineering 89 (11) (2012) 1419–1436. doi:10.1002/nme.3295.

[9] J. Zeman, J. Vondřejc, J. Novák, I. Marek, Accelerating a FFT-based solver for numerical homogenization of periodic media by conjugate gradients, Journal of Computational Physics 229 (21) (2010) 8065–8071. doi:10.1016/j.jcp.2010.07.010.

[10] S. Brisard, L. Dormieux, FFT-based methods for the mechanics of composites: A general variational framework, Computational Materials Science 49 (3) (2010) 663–671. doi:10.1016/j.commatsci.2010.06.009.

[11] L. Gélébart, R. Mondon-Cancel, Non-linear extension of FFT-based methods accelerated by conjugate gradients to evaluate the mechanical behavior of composite materials, Computational Materials Science 77 (2013) 430–439. doi:10.1016/j.commatsci.2013.04.046.

[12] M. Kabel, T. Böhlke, M. Schneider, Efficient fixed point and Newton–Krylov solvers for FFT-based homogenization of elasticity at large deformations, Computational Mechanics 54 (6) (2014) 1497–1514. doi:10.1007/s00466-014-1071-8.

[13] M. Schneider, An FFT-based fast gradient method for elastic and inelastic unit cell homogenization problems, Computer Methods in Applied Mechanics and Engineering 315 (2017) 846–866. doi:10.1016/j.cma.2016.11.004.

[14] M. Schneider, On the Barzilai-Borwein basic scheme in FFT-based computational homogenization, International Journal for Numerical Methods in Engineering 118 (8) (2019) 482–494. doi:10.1002/nme.6023.
[15] M. Schneider, A review of nonlinear FFT-based computational homogenization methods, Acta Mechanica 232 (6) (2021) 2051–2100. doi:10.1007/s00707-021-02962-1.
[16] H. Moulinec, F. Silva, Comparison of three accelerated FFT-based schemes for computing the mechanical response of composite materials, International Journal for Numerical Methods in Engineering 97 (13) (2014) 960–985. doi:10.1002/nme.4614.
[17] M. Schneider, D. Wicht, T. Böhlke, On polarization-based schemes for the FFT-based computational homogenization of inelastic materials, Computational Mechanics 64 (4) (2019) 1073–1095. doi:10.1007/s00466-019-01694-3.
[18] G. W. Milton, The Theory of Composites, no. 6 in Cambridge Monographs on Applied and Computational Mathematics, Cambridge University Press, Cambridge; New York, 2002.
[19] T. Mura, Micromechanics of Defects in Solids, 2nd Edition, no. 3 in Mechanics of Elastic and Inelastic Solids, Kluwer Academic Publishers, 1987.
[20] P. Suquet, A simplified method for the prediction of homogenized elastic properties of composites with a periodic structure, Comptes-rendus de l'Académie des sciences série II 311 (7) (1990) 769–774.
[21] C. Bellis, P. Suquet, Geometric variational principles for computational homogenization, Journal of Elasticity 137 (2019) 119–149. doi:10.1007/s10659-018-09713-9.
[22] H. Moulinec, P. Suquet, G. Milton, Convergence of iterative methods based on Neumann series for composite materials: Theory and practice, International Journal for Numerical Methods in Engineering (2018) 1–28.
[23] J. Moreau, Duality characterization of strain tensor distributions in an arbitrary open set, Journal of Mathematical Analysis and Applications 72 (2) (1979) 760–770. doi:10.1016/0022-247X(79)90263-4.
[24] M. Schneider, Lippmann-Schwinger solvers for the computational homogenization of materials with pores, International Journal for Numerical Methods in Engineering 121 (22) (2020) 5017–5041.
[25] F. Willot, Fourier-based schemes for computing the mechanical response of composites with accurate local fields, Comptes Rendus Mécanique 343 (3) (2015) 232–245.
[26] K. Sab, J. Bleyer, S. Brisard, M. Dolbeau, Supplementary material to "An FFT-based adaptive polarization method for infinitely contrasted media with guaranteed convergence" (Mar. 2024). doi:10.5281/zenodo.10852953.
URL https://doi.org/10.5281/zenodo.10852953

A. On the formulation of the accelerated scheme of Eyre and Milton

In this section, we prove that formulations (24) and (32) are equivalent. We first recognize in the iterations (24) the residual $\boldsymbol{X}^n$ defined by Eq. (30) and get the following formulation, equivalent to (24)

$$\begin{cases} \textbf{Initialization} \\ \boldsymbol{\varepsilon}^0 = \boldsymbol{E} \end{cases} \quad \text{and} \quad \begin{cases} \textbf{Iterations } (n \geq 0) \\ \boldsymbol{X}^n = \boldsymbol{E} - \boldsymbol{\varepsilon}^n - \boldsymbol{\Gamma}^0 * [(\boldsymbol{C} - \boldsymbol{C}_0) : \boldsymbol{\varepsilon}^n] \\ \boldsymbol{\varepsilon}^{n+1} = \boldsymbol{\varepsilon}^n + \boldsymbol{\alpha} : \boldsymbol{X}^n \end{cases} \tag{A.1}$$

Definition (30) reads, for $\boldsymbol{X}^{n+1}$

$$\boldsymbol{X}^{n+1} = \boldsymbol{E} - \boldsymbol{\varepsilon}^{n+1} - \boldsymbol{\Gamma}^0 * [(\boldsymbol{C} - \boldsymbol{C}_0) : \boldsymbol{\varepsilon}^{n+1}] \tag{A.2}$$

and plugging $\boldsymbol{\varepsilon}^{n+1} = \boldsymbol{\varepsilon}^n + \boldsymbol{\alpha} : \boldsymbol{X}^n$

$$\begin{aligned} \boldsymbol{X}^{n+1} &= \boldsymbol{E} - \boldsymbol{\varepsilon}^n - \boldsymbol{\alpha} : \boldsymbol{X}^n - \boldsymbol{\Gamma}^0 * [(\boldsymbol{C} - \boldsymbol{C}_0) : \boldsymbol{\varepsilon}^n + (\boldsymbol{C} - \boldsymbol{C}_0) : \boldsymbol{\alpha} : \boldsymbol{X}^n] \\ &= \boldsymbol{E} - \boldsymbol{\varepsilon}^n - \boldsymbol{\Gamma}^0 * [(\boldsymbol{C} - \boldsymbol{C}_0) : \boldsymbol{\varepsilon}^n] - \boldsymbol{\alpha} : \boldsymbol{X}^n - \boldsymbol{\Gamma}^0 * [(\boldsymbol{C} - \boldsymbol{C}_0) : \boldsymbol{\alpha} : \boldsymbol{X}^n] \end{aligned} \tag{A.3}$$

finally, recognizing the definition (30) of $\boldsymbol{X}^n$

$$\boldsymbol{X}^{n+1} = \boldsymbol{X}^n - \boldsymbol{\alpha} : \boldsymbol{X}^n - \boldsymbol{\Gamma}^0 * [(\boldsymbol{C} - \boldsymbol{C}_0) : \boldsymbol{\alpha} : \boldsymbol{X}^n] \tag{A.4}$$

we get the following equivalent formulation of the accelerated scheme (24)

$$\begin{cases} \textbf{Initialization} \\ \boldsymbol{\varepsilon}^0 = \boldsymbol{E} \\ \boldsymbol{X}^0 = -\boldsymbol{\Gamma}^0 * [(\boldsymbol{C} - \boldsymbol{C}_0) : \boldsymbol{E}] \end{cases} \quad \text{and} \quad \begin{cases} \textbf{Iterations } (n \geq 0) \\ \boldsymbol{\varepsilon}^{n+1} = \boldsymbol{\varepsilon}^n + \boldsymbol{\alpha} : \boldsymbol{X}^n \\ \boldsymbol{X}^{n+1} = \boldsymbol{X}^n - \boldsymbol{\alpha} : \boldsymbol{X}^n - \boldsymbol{\Gamma}^0 * [(\boldsymbol{C} - \boldsymbol{C}_0) : \boldsymbol{\alpha} : \boldsymbol{X}^n] \end{cases} \tag{A.5}$$

and formulation (32) is finally retrieved.

B. Proof of Eqs. (39), (40) and (66)

In this appendix, a proof of the bounds (39) and (40) on $\boldsymbol{e} : \boldsymbol{C}^D(\boldsymbol{y}) : \boldsymbol{e}$ and $\boldsymbol{e} : \boldsymbol{C}^S(\boldsymbol{y}) : \boldsymbol{e}$ is proposed. It will be convenient to introduce the following partial order relation $\preccurlyeq$ over the space of fourth-order, positive definite tensors with major and minor symmetries

$$\boldsymbol{T} \preccurlyeq \boldsymbol{T} \quad \Longleftrightarrow \quad \boldsymbol{e} : \boldsymbol{T} : \boldsymbol{e} \leq \boldsymbol{e} : \boldsymbol{T}' : \boldsymbol{e}, \tag{B.1}$$

for all second-order, symmetric tensors $\boldsymbol{e}$. Then, the uniform coercivity condition reads

$$\mu^- \boldsymbol{C}_0 \preccurlyeq \boldsymbol{C}(\boldsymbol{y}) \preccurlyeq \mu^+ \boldsymbol{C}_0, \tag{B.2}$$

for all $\boldsymbol{y} \in \Omega$. The partial order relation $\preccurlyeq$ has the following properties[3]

1. $\boldsymbol{T} \preccurlyeq \boldsymbol{T} \quad \Rightarrow \quad \lambda \boldsymbol{T} \leq \lambda \boldsymbol{T}' \quad$ for all $\quad \lambda > 0$,
2. $(\boldsymbol{T}_1 \preccurlyeq \boldsymbol{T}_1' \quad \text{and} \quad \boldsymbol{T}_2 \preccurlyeq \boldsymbol{T}_2') \quad \Rightarrow \quad \boldsymbol{T}_1 + \boldsymbol{T}_2 \preccurlyeq \boldsymbol{T}_1' + \boldsymbol{T}_2'$,
3. $\boldsymbol{T} \preccurlyeq \boldsymbol{T}' \quad \Rightarrow \quad \boldsymbol{T}'^{-1} \preccurlyeq \boldsymbol{T}^{-1}$,

from which it results

$$\begin{aligned}
& \mu^- \boldsymbol{C}_0 \preccurlyeq \boldsymbol{C}(\boldsymbol{y}) \preccurlyeq \mu^+ \boldsymbol{C}_0, \\
\Rightarrow \quad & \mu^- \boldsymbol{C}_0 + \boldsymbol{C}_0 \preccurlyeq \boldsymbol{C}(\boldsymbol{y}) + \boldsymbol{C}_0 \preccurlyeq \mu^+ \boldsymbol{C}_0 + \boldsymbol{C}_0, \\
\Rightarrow \quad & (\mu^+ + 1)^{-1} \boldsymbol{C}_0^{-1} \preccurlyeq (\boldsymbol{C}(\boldsymbol{y}) + \boldsymbol{C}_0)^{-1} \preccurlyeq (\mu^- + 1)^{-1} \boldsymbol{C}_0^{-1}, \\
\Rightarrow \quad & 2(\mu^+ + 1)^{-1} \boldsymbol{C}_0 \preccurlyeq \boldsymbol{C}^S(\boldsymbol{y}) \preccurlyeq 2(\mu^- + 1)^{-1} \boldsymbol{C}_0,
\end{aligned} \tag{B.3}$$

Inequality (39) is a consequence of the identity (38).

In order to prove the last inequality in (66), we will establish $\boldsymbol{C}^S : \boldsymbol{C}_0^{-1} : \boldsymbol{C}^S \preccurlyeq 4\boldsymbol{C}_0$ and $\boldsymbol{C}^D : \boldsymbol{C}_0^{-1} : \boldsymbol{C}^D \preccurlyeq 4\boldsymbol{C}_0$. Simple algebraic calculations lead to to the following expression of $\boldsymbol{C}^S : \boldsymbol{C}_0^{-1} : \boldsymbol{C}^S$ and $\boldsymbol{C}^D : \boldsymbol{C}_0^{-1} : \boldsymbol{C}^D$ in the matrix:

$$\boldsymbol{C}^S(\boldsymbol{y}) : \boldsymbol{C}_0^{-1} : \boldsymbol{C}^S(\boldsymbol{y}) = 4\boldsymbol{C}_0 : (\boldsymbol{C}(\boldsymbol{y}) : \boldsymbol{C}_0^{-1} : \boldsymbol{C}(\boldsymbol{y}) + 2\boldsymbol{C}(\boldsymbol{y}) + \boldsymbol{C}_0)^{-1} : \boldsymbol{C}_0 \tag{B.4}$$

and

$$\boldsymbol{C}^D(\boldsymbol{y}) : \boldsymbol{C}_0^{-1} : \boldsymbol{C}^D(\boldsymbol{y}) = 4\boldsymbol{C}_0 : (\boldsymbol{C}_0 : \boldsymbol{C}^{-1}(\boldsymbol{y}) : \boldsymbol{C}_0 : \boldsymbol{C}^{-1}(\boldsymbol{y}) : \boldsymbol{C}_0 + 2\boldsymbol{C}_0 : \boldsymbol{C}^{-1}(\boldsymbol{y}) : \boldsymbol{C}_0 + \boldsymbol{C}_0)^{-1} : \boldsymbol{C}_0. \tag{B.5}$$

From the positivity of $\boldsymbol{C}(\boldsymbol{y})$ and $\boldsymbol{C}_0$ it results

$$\begin{aligned}
& \boldsymbol{C}_0 \preccurlyeq \boldsymbol{C}(\boldsymbol{y}) : \boldsymbol{C}_0^{-1} : \boldsymbol{C}(\boldsymbol{y}) + 2\boldsymbol{C}(\boldsymbol{y}) + \boldsymbol{C}_0, \\
\Rightarrow \quad & (\boldsymbol{C}(\boldsymbol{y}) : \boldsymbol{C}_0^{-1} : \boldsymbol{C}(\boldsymbol{y}) + 2\boldsymbol{C}(\boldsymbol{y}) + \boldsymbol{C}_0)^{-1} \preccurlyeq \boldsymbol{C}_0^{-1} \\
\Rightarrow \quad & \boldsymbol{C}^S(\boldsymbol{y}) : \boldsymbol{C}_0^{-1} : \boldsymbol{C}^S(\boldsymbol{y}) \preccurlyeq 4\boldsymbol{C}_0
\end{aligned} \tag{B.6}$$

and

$$\begin{aligned}
& \boldsymbol{C}_0 \preccurlyeq \boldsymbol{C}_0 : \boldsymbol{C}^{-1}(\boldsymbol{y}) : \boldsymbol{C}_0 : \boldsymbol{C}^{-1}(\boldsymbol{y}) : \boldsymbol{C}_0 + 2\boldsymbol{C}_0 : \boldsymbol{C}^{-1}(\boldsymbol{y}) : \boldsymbol{C}_0 + \boldsymbol{C}_0, \\
\Rightarrow \quad & (\boldsymbol{C}_0 : \boldsymbol{C}^{-1}(\boldsymbol{y}) : \boldsymbol{C}_0 : \boldsymbol{C}^{-1}(\boldsymbol{y}) : \boldsymbol{C}_0 + 2\boldsymbol{C}_0 : \boldsymbol{C}^{-1}(\boldsymbol{y}) : \boldsymbol{C}_0 + \boldsymbol{C}_0)^{-1} \preccurlyeq \boldsymbol{C}_0^{-1} \\
\Rightarrow \quad & \boldsymbol{C}^D(\boldsymbol{y}) : \boldsymbol{C}_0^{-1} : \boldsymbol{C}^D(\boldsymbol{y}) \preccurlyeq 4\boldsymbol{C}_0
\end{aligned} \tag{B.7}$$

Finally, we have $\boldsymbol{C}^S : \boldsymbol{C}_0^{-1} : \boldsymbol{C}^S = 0$ and $\boldsymbol{C}^D : \boldsymbol{C}_0^{-1} : \boldsymbol{C}^D = 4\boldsymbol{C}_0$ in the rigid inclusions, while $\boldsymbol{C}^S : \boldsymbol{C}_0^{-1} : \boldsymbol{C}^S = 4\boldsymbol{C}_0$ and $\boldsymbol{C}^D : \boldsymbol{C}_0^{-1} : \boldsymbol{C}^D = 0$ in the pores.

[3] Note that the proof of the last property results from the fact that $\frac{1}{2}\,\boldsymbol{\sigma} : \boldsymbol{T} : \boldsymbol{\sigma} = \max_{\boldsymbol{e}} \left\{ \boldsymbol{\sigma} : \boldsymbol{e} - \frac{1}{2}\,\boldsymbol{e} : \boldsymbol{T} : \boldsymbol{e} \right\}$.

C. On the regularity of Ω^{r}

The case of several rigid inclusions occupying Ω-periodic non-intersection Lipschitz domains is a simple extension of the case we consider here of one single inclusion occupying a Lipschitz domain $\Omega^{\mathrm{r}} \subset \Omega$ and such that its boundary $\partial\Omega^{\mathrm{r}}$ is in the interior of Ω.

Let $\boldsymbol{e}$ be in $\boldsymbol{L}^2_{\mathrm{sym}}(\Omega)$ such that $\boldsymbol{C}_0 : \boldsymbol{e} \in \boldsymbol{S}^r$. This means that the divergence of $\boldsymbol{C}_0 : \boldsymbol{e}$ is null and that $\boldsymbol{e}$ in Ω^{r} is equal to the symmetric part of the gradient of some displacement vector field on Ω^{r}. The divergence of $\boldsymbol{C}_0 : \boldsymbol{e}$ being null, its normal trace on $\partial\Omega^{\mathrm{r}}$, noted $\gamma_n(\boldsymbol{C}_0 : \boldsymbol{e})$, where $\boldsymbol{n}$ is the outer normal to $\partial\Omega^{\mathrm{r}}$, is well-defined in $H^{-\frac{1}{2}}(\partial\Omega^{\mathrm{r}})$. The displacement field in Ω^{r} that generates the restriction of $\boldsymbol{e}$ to Ω^{r} as the symmetric part of its gradient is uniquely defined up to a rigid-body-like displacement, and it is in $H^1(\Omega^{\mathrm{r}})^d$. We choose among all these possible displacement fields the one which minimizes the H^1-norm in Ω^{r}, which we note $\boldsymbol{u}$. Then, the trace of $\boldsymbol{u}$ on $\partial\Omega^{\mathrm{r}}$, noted $\gamma_0(\boldsymbol{u})$, is also well-defined and it is in $H^{+\frac{1}{2}}(\partial\Omega^{\mathrm{r}})$. Using the Stokes formula, we have:

$$\int_{\Omega^{\mathrm{r}}} \boldsymbol{e} : \boldsymbol{C}_0 : \boldsymbol{e} = (\gamma_n(\boldsymbol{C}_0 : \boldsymbol{e}), \gamma_0(\boldsymbol{u})) \leq \|\gamma_n(\boldsymbol{C}_0 : \boldsymbol{e})\|_{H^{-\frac{1}{2}}(\partial\Omega^{\mathrm{r}})} \|\gamma_0(\boldsymbol{u})\|_{H^{+\frac{1}{2}}(\partial\Omega^{\mathrm{r}})} \tag{C.1}$$

Here, $(.,.)$ denotes the duality operator between the dual spaces $H^{-\frac{1}{2}}(\partial\Omega^{\mathrm{r}})$ and $H^{+\frac{1}{2}}(\partial\Omega^{\mathrm{r}})$ and if $\boldsymbol{e}$ and $\boldsymbol{u}$ are regular enough, we have:

$$(\gamma_n(\boldsymbol{C}_0 : \boldsymbol{e}), \gamma_0(\boldsymbol{u})) = \int_{\partial\Omega^{\mathrm{r}}} [(\boldsymbol{C}_0 : \boldsymbol{e}) \cdot \boldsymbol{n}] \cdot \boldsymbol{u} \tag{C.2}$$

From the continuity of the trace operator from $H^1(\Omega^{\mathrm{r}})^d$ into $H^{+\frac{1}{2}}(\partial\Omega^{\mathrm{r}})$, and from the Korn inequality which states that the H^1-norm of the displacement field $\boldsymbol{u}$ in Ω^{r} is equivalent to the L^2-norm of its corresponding strain field in Ω^{r}, $\boldsymbol{e}$, we conclude that there is a constant $c_1 > 0$, independent of $\boldsymbol{e}$, such that:

$$\|\gamma_0(\boldsymbol{u})\|^2_{H^{+\frac{1}{2}}(\partial\Omega^{\mathrm{r}})} \leq c_1 \int_{\Omega^{\mathrm{r}}} \boldsymbol{e} : \boldsymbol{C}_0 : \boldsymbol{e} \tag{C.3}$$

Hence, we have:

$$\int_{\Omega^{\mathrm{r}}} \boldsymbol{e} : \boldsymbol{C}_0 : \boldsymbol{e} \leq c_1 \|\gamma_n(\boldsymbol{C}_0 : \boldsymbol{e})\|^2_{H^{-\frac{1}{2}}(\partial\Omega^{\mathrm{r}})} \tag{C.4}$$

Now we consider the restriction of $\boldsymbol{C}_0 : \boldsymbol{e}$ to $\Omega \setminus \Omega^{\mathrm{r}}$. It is in $\boldsymbol{L}^2_{\mathrm{sym}}(\Omega \setminus \Omega^{\mathrm{r}})$ and divergence-free. Hence, its normal trace is well-defined on the boundary of $\Omega \setminus \Omega^{\mathrm{r}}$, $\partial\Omega^{\mathrm{r}} \cup \partial\Omega$. Then, noticing that the outer normal $\boldsymbol{m}$ to the boundary of $\Omega \setminus \Omega^{\mathrm{r}}$ coincides with $-\boldsymbol{n}$ on $\partial\Omega^{\mathrm{r}}$ and by the continuity of the trace operator from the subspace of divergence-free elements in $\boldsymbol{L}^2_{\mathrm{sym}}(\Omega \setminus \Omega^{\mathrm{r}})$ into $H^{-\frac{1}{2}}(\partial\Omega^{\mathrm{r}} \cup \partial\Omega)$, we have:

$$\|\gamma_n(\boldsymbol{C}_0 : \boldsymbol{e})\|^2_{H^{-\frac{1}{2}}(\partial\Omega^{\mathrm{r}})} \leq \|\gamma_m(\boldsymbol{C}_0 : \boldsymbol{e})\|^2_{H^{-\frac{1}{2}}(\partial\Omega^{\mathrm{r}} \cup \partial\Omega)} \leq c_2 \int_{\Omega \setminus \Omega^{\mathrm{r}}} \boldsymbol{e} : \boldsymbol{C}_0 : \boldsymbol{e} \tag{C.5}$$

where $c_2 > 0$ is a positive constant independent of $\boldsymbol{e}$. Hence, the claimed property is proved with $c = 1 + c_1 c_2 > 0$.

D. On the regularity of Ω^{p}

The case of pores occupying Ω-periodic non-intersection Lipschitz domains is a simple extension of the case we consider here of one single pore occupying a Lipschitz domain $\Omega^{\mathrm{p}} \subset \Omega$ and such that its boundary $\partial\Omega^{\mathrm{p}}$ is in the interior of Ω.

Let $\boldsymbol{e}$ be in $\boldsymbol{D}^p$, which means that it is in $\boldsymbol{D}$ and $\boldsymbol{C}_0 : \boldsymbol{e}$ is divergence-free in Ω^{p}. Similarly to the previous appendix, using an appropriate Stokes formula on this Dirichlet elasticity problem in Ω^{p}, and the continuity of the trace operators on its boundary, enables us to show that:

$$\int_{\Omega^{\mathrm{p}}} \boldsymbol{e} : \boldsymbol{C}_0 : \boldsymbol{e} \leq c_1 \|\gamma_0(\boldsymbol{u})\|^2_{H^{+\frac{1}{2}}(\partial\Omega^{\mathrm{p}})} \tag{D.1}$$

The proof is ended thanks to the Korn's inequality in $\Omega \setminus \Omega^{\mathrm{p}}$ and the continuity of the trace operator on the boundary of this domain.

E. The gradient of potential J

Let $\boldsymbol{\varepsilon}^*$ and $\delta\boldsymbol{\varepsilon}^*$ be in $\boldsymbol{L}^2_{\text{sym}}(\Omega)$. Then, $\nabla J(\boldsymbol{\varepsilon}^*)$ is by definition such that:

$$\lim_{\lambda\to 0}\frac{J(\boldsymbol{\varepsilon}^*+\lambda\delta\boldsymbol{\varepsilon}^*)-J(\boldsymbol{\varepsilon}^*)}{\lambda}=\langle\nabla J(\boldsymbol{\varepsilon}^*):\boldsymbol{C}_0:\delta\boldsymbol{\varepsilon}^*\rangle_\Omega \tag{E.1}$$

From equations (95), (90) and (64), we can rewrite J as following:

$$J(\boldsymbol{\varepsilon}^*)=\frac{1}{2}\langle(E-\boldsymbol{\alpha}:\boldsymbol{\varepsilon}^*)^S:\boldsymbol{C}_0:(E-\boldsymbol{\alpha}:\boldsymbol{\varepsilon}^*)^S\rangle_\Omega+\frac{1}{2}\langle((2\boldsymbol{I}-\boldsymbol{\alpha}):\boldsymbol{\varepsilon}^*)^D:\boldsymbol{C}_0:((2\boldsymbol{I}-\boldsymbol{\alpha}):\boldsymbol{\varepsilon}^*)^D\rangle_\Omega \tag{E.2}$$

From the definition (E.1), we obtain:

$$\langle\nabla J(\boldsymbol{\varepsilon}^*):\boldsymbol{C}_0:\delta\boldsymbol{\varepsilon}^*\rangle_\Omega=\langle(E-\boldsymbol{\alpha}:\boldsymbol{\varepsilon}^*)^S:\boldsymbol{C}_0:(-\boldsymbol{\alpha}:\delta\boldsymbol{\varepsilon}^*)^S\rangle_\Omega+\langle((2\boldsymbol{I}-\boldsymbol{\alpha}):\boldsymbol{\varepsilon}^*)^D:\boldsymbol{C}_0:((2\boldsymbol{I}-\boldsymbol{\alpha}):\delta\boldsymbol{\varepsilon}^*)^D\rangle_\Omega \tag{E.3}$$

and thanks to orthogonality:

$$\langle\nabla J(\boldsymbol{\varepsilon}^*):\boldsymbol{C}_0:\delta\boldsymbol{\varepsilon}^*\rangle_\Omega=\langle(E-\boldsymbol{\alpha}:\boldsymbol{\varepsilon}^*)^S:\boldsymbol{C}_0:(-\boldsymbol{\alpha}:\delta\boldsymbol{\varepsilon}^*)\rangle_\Omega+\langle((2\boldsymbol{I}-\boldsymbol{\alpha}):\boldsymbol{\varepsilon}^*)^D:\boldsymbol{C}_0:((2\boldsymbol{I}-\boldsymbol{\alpha}):\delta\boldsymbol{\varepsilon}^*)\rangle_\Omega \tag{E.4}$$

Now, using the symmetry of $\boldsymbol{C}^S$, $\boldsymbol{C}^S=\boldsymbol{C}_0:\boldsymbol{\alpha}=\boldsymbol{\alpha}^t:\boldsymbol{C}_0$, we can identify $\nabla J(\boldsymbol{\varepsilon}^*)$ as:

$$\nabla J(\boldsymbol{\varepsilon}^*)=-\boldsymbol{\alpha}:(E-\boldsymbol{\alpha}:\boldsymbol{\varepsilon}^*)^S+(2\boldsymbol{I}-\boldsymbol{\alpha}):((2\boldsymbol{I}-\boldsymbol{\alpha}):\boldsymbol{\varepsilon}^*)^D \tag{E.5}$$

and

$$\nabla J(\boldsymbol{\varepsilon}^*)=-\boldsymbol{\alpha}:E+\boldsymbol{\alpha}:(\boldsymbol{\alpha}:\boldsymbol{\varepsilon}^*)^S+(2\boldsymbol{I}-\boldsymbol{\alpha}):((2\boldsymbol{\varepsilon}^*)^D-(\boldsymbol{\alpha}:\boldsymbol{\varepsilon}^*)^D) \tag{E.6}$$

Using the orthogonal decomposition $(\boldsymbol{\alpha}:\boldsymbol{\varepsilon}^*)^S+(\boldsymbol{\alpha}:\boldsymbol{\varepsilon}^*)^D=\boldsymbol{\alpha}:\boldsymbol{\varepsilon}^*$ in the above equation finally leads to the following expression of $\nabla J(\boldsymbol{\varepsilon}^*)$: We have the following expression:

$$\nabla J(\boldsymbol{\varepsilon}^*)=\boldsymbol{\alpha}^2:\boldsymbol{\varepsilon}^*+(4\boldsymbol{I}-2\boldsymbol{\alpha}):(\boldsymbol{\varepsilon}^*)^D-2(\boldsymbol{\alpha}:\boldsymbol{\varepsilon}^*)^D-\boldsymbol{\alpha}:E. \tag{E.7}$$

Actually, we can express ∇J in terms of the operator Z defined by equation (61) and its transpose Z^t defined by:

$$\langle\boldsymbol{X}_1:\boldsymbol{C}_0:\boldsymbol{Z}(\boldsymbol{X}_2)\rangle_\Omega=\langle\boldsymbol{X}_2:\boldsymbol{C}_0:\boldsymbol{Z}^t(\boldsymbol{X}_1)\rangle_\Omega \tag{E.8}$$

for any $\boldsymbol{X}_1$ and $\boldsymbol{X}_2$ be in $\boldsymbol{L}^2_{\text{sym}}(\Omega)$. Then, we have:

$$\boldsymbol{Z}^t(\boldsymbol{X})=\boldsymbol{\alpha}:\boldsymbol{X}+2(\boldsymbol{I}-\boldsymbol{\alpha}):\boldsymbol{X}^D, \tag{E.9}$$

and

$$\nabla J(\boldsymbol{\varepsilon}^*)=\boldsymbol{Z}^t(\boldsymbol{Z}(\boldsymbol{\varepsilon}^*))-\boldsymbol{Z}^t(E)=\boldsymbol{Z}^t(\boldsymbol{Z}(\boldsymbol{\varepsilon}^*)-E). \tag{E.10}$$

F. Another version of the AEM scheme

The computation of the compatibility and equilibrium residuals Δ^S and Δ^D introduced in (106) and (107) requires to compute the projections $\boldsymbol{\varepsilon}^S$ and $\left(\boldsymbol{C}_0^{-1}:\boldsymbol{\sigma}\right)^D$. From the residual decomposition (50), we have $\left(\boldsymbol{C}_0^{-1}:\boldsymbol{\sigma}\right)^D=-\boldsymbol{X}^D$. The algorithm is started with a chosen pair of strain-stress fields in the unit-cell $(\boldsymbol{\varepsilon}^0,\boldsymbol{\sigma}^0)$ verifying (46). Its corresponding residual $\boldsymbol{X}^0$, as well as the projections $(\boldsymbol{\varepsilon}^0)^S$ and $(\boldsymbol{X}^0)^D$ are computed. For instance, the zero initialization is given by: $\boldsymbol{\varepsilon}^0=0$, $\boldsymbol{\sigma}^0=0$, $\boldsymbol{X}^0=\boldsymbol{E}$, $(\boldsymbol{\varepsilon}^0)^S=0$ and $(\boldsymbol{X}^0)^D=0$.

For $n \geq 0$, if $\boldsymbol{X}^n = 0$ then the pair $(\boldsymbol{\varepsilon}^n, \boldsymbol{\sigma}^n)$ is a solution of the homogenization problem and the iteration is stopped. Otherwise, compute $\boldsymbol{\varepsilon}^{n+1}$, $\boldsymbol{\sigma}^{n+1}$, $\boldsymbol{X}^{n+1}$, $(\boldsymbol{\varepsilon}^{n+1})^S$ and $\left(\boldsymbol{X}^{n+1}\right)^D$, as follows:

$$\boldsymbol{Y}^n = \boldsymbol{\alpha} : \boldsymbol{X}^n \tag{F.1}$$

$$(\boldsymbol{Y}^n)^D = \boldsymbol{\Gamma}^0 * (\boldsymbol{C}_0 : \boldsymbol{Y}^n) \tag{F.2}$$

$$(\boldsymbol{Y}^n)^S = \boldsymbol{Y}^n - (\boldsymbol{Y}^n)^D \tag{F.3}$$

$$(\boldsymbol{Z}^n)^D = 2\,(\boldsymbol{X}^n)^D - (\boldsymbol{Y}^n)^D \tag{F.4}$$

$$\boldsymbol{Z}^n = (\boldsymbol{Y}^n)^S + (\boldsymbol{Z}^n)^D \tag{F.5}$$

$$\lambda^n = \frac{\langle \boldsymbol{X}^n : \boldsymbol{C}_0 : \boldsymbol{Z}^n \rangle_\Omega}{\langle \boldsymbol{Z}^n : \boldsymbol{C}_0 : \boldsymbol{Z}^n \rangle_\Omega} \tag{F.6}$$

$$\boldsymbol{X}^{n+1} = \boldsymbol{X}^n - \lambda^n \boldsymbol{Z}^n \tag{F.7}$$

$$\boldsymbol{\varepsilon}^{n+1} = \boldsymbol{\varepsilon}^n + \lambda^n \boldsymbol{Y}^n \tag{F.8}$$

$$\boldsymbol{\sigma}^{n+1} = \boldsymbol{\sigma}^n + \lambda^n \boldsymbol{C}^D : \boldsymbol{X}^n. \tag{F.9}$$

$$(\boldsymbol{\varepsilon}^{n+1})^S = (\boldsymbol{\varepsilon}^n)^S + \lambda^n\,(\boldsymbol{Y}^n)^S \tag{F.10}$$

$$\left(\boldsymbol{X}^{n+1}\right)^D = (\boldsymbol{X}^n)^D - \lambda^n\,(\boldsymbol{Z}^n)^D\,. \tag{F.11}$$

Indeed, this scheme is equivalent to the original one and it enables us to compute both residuals Δ^S and Δ^D from $\boldsymbol{X}^D$ and $\boldsymbol{X}^S$. To see this, one can notice from the Z-decomposition (61) and the property (38) that $\boldsymbol{Z} = \boldsymbol{Y} + 2\boldsymbol{X}^D - 2\boldsymbol{Y}^D = \boldsymbol{Y}^S + 2\boldsymbol{X}^D - \boldsymbol{Y}^D$ where $\boldsymbol{Y} = \boldsymbol{\alpha} : \boldsymbol{X}$.